SAND2024-00538J

Large-scale Harmonic Balance Simulations with Krylov Subspace and Preconditioner Recycling

Robert J. Kuether[1], Andrew Steyer[1]

[1] Sandia National Laboratories, Albuquerque, NM, USA

ABSTRACT

The multi-harmonic balance method combined with numerical continuation provides an efficient framework to compute a family of time-periodic solutions, or response curves, for large-scale, nonlinear mechanical systems. The predictor and corrector steps repeatedly solve a sequence of linear systems that scale by the model size and number of harmonics in the assumed Fourier series approximation. In this paper, a novel Newton-Krylov iterative method is embedded within the multi-harmonic balance and continuation algorithm to efficiently compute the approximate solutions from the sequence of linear systems that arise during the prediction and correction steps. The method recycles, or re-uses, both the preconditioner and the Krylov subspace generated by previous linear systems in the solution sequence. A delayed frequency preconditioner refactorizes the preconditioner only when the performance of the iterative solver deteriorates. The GCRO-DR iterative solver recycles a subset of harmonic Ritz vectors to initialize the solution subspace for the next linear system in the sequence. The performance of the iterative solver is demonstrated on two exemplars with contact-type nonlinearities and benchmarked against a direct solver with traditional Newton-Raphson iterations.

Keywords: *periodic orbits; multi-harmonic balance; Newton-Krylov; delayed frequency preconditioner; Krylov subspace recycling*

1. Introduction

Linear system theory has served as the cornerstone for analytical, computational, and experimental structural dynamics analysis for decades. Modal analysis of linear systems benefits from the property of orthogonality and superposition to decompose the response into the modal domain and treat vibrations as a summation of single degree-of-freedom (DOF) oscillators. Frequency response functions (FRFs) provide an invariant relationship between the excitation and response in the frequency domain thanks to homogeneity. Both mathematical models rely on the computation of periodic motions of the linear dynamical system. These foundational techniques necessitate linear approximations of the physics to mathematically model the vibration response with linear system theory. In practice, the linearity assumption may not be valid or justifiable. Structural nonlinearities persist across many engineering disciplines including aerospace, automotive, civil, and biomedical engineering. These nonlinearities arise from the presence of large deflections, frictional contact, or nonlinear material behavior, for example. Nonlinear dynamical systems demand the use of alternate mathematical models and solution methods [1] to predict response.

The study of periodic orbits is important in understanding the behavior of nonlinear dynamical systems. There are many classifications describing the type of time-periodic solutions, whether the system is autonomous or non-autonomous, and conservative or non-conservative. Examples of these include nonlinear normal modes (NNMs) [2, 3], limit cycle oscillations [4, 5] and nonlinear forced response (NLFR) curves [6]. Several analytical and computational techniques are available to calculate the time-periodic solutions of a nonlinear system including perturbation methods [7], averaging methods, harmonic balance [8], shooting [9, 10], and orthogonal collocation. In the age of digital engineering, the development of computational methods to compute the time-periodic solutions are needed, especially for large-scale computational mechanics models. The multi-harmonic balance (MHB) method provides a promising technique to efficiently calculate time-periodic solutions of the spatially

[2] Sandia National Laboratories is a multimission laboratory managed and operated by National Technology & Engineering Solutions of Sandia, LLC, a wholly owned subsidiary of Honeywell International Inc., for the U.S. Department of Energy's National Nuclear Security Administration under contract DE-NA0003525.

discretized equations-of-motion resulting from the finite element method. MHB approximates the assumed time-periodic response with a finite Fourier series. The Fourier-Galerkin projection onto the nonlinear ordinary differential equation results in a nonlinear algebraic system, which is solved for the unknown Fourier coefficients. When the nonlinear algebraic equations are combined with numerical continuation [11, 12], a family of periodic orbits is computed to produce a branch of solutions that characterize the dynamics of the system. Typically MHB and continuation provide an adequate approximation to the time-periodic solutions for both smooth [13] and non-smooth [14] systems depending on the number of harmonics in the Fourier series.

Many researchers have utilized MHB with continuation to compute periodic orbits of nonlinear systems. Example include MHB for vibration problems, as discussed in the book by Krack and Gross [8], and applications to nonlinear electromagnetics [15]. For nonlinear vibration problems, MHB has found applications in rotating machinery [16-19], bladed disks [20-24], vibro-impact systems [25-29] and large deformation problems [30-34]. These references highlight the generalization of the approach to structural models with different forms of nonlinear physics. The alternating frequency-time (AFT) domain method [35] enables arbitrary nonlinear internal forces to be discretely sampled in the time domain and mapped into the frequency domain using the Fourier transform. For example, the papers by Detroux et al. [36] and Colaitis et al. [21] provide details of the computation of the nonlinear forces and Jacobians in the frequency domain using an adaptation of AFT using trigonometric collocation [37, 38]. Other approaches include analytical derivations of the nonlinear forces and Jacobians in the frequency domain, e.g. friction elements [39], but may be in general limited to certain types of nonlinearity and harmonic order. Although MHB is efficient and generalized to arbitrary types of nonlinearity, one notable challenge is the issue of scalability to large-scale systems, as noted in [40]. The system of equations derived from MHB scale linearly with the number of harmonics in the Fourier series, and thus the resultant linear systems become quite large for finite element models with many DOF and many harmonics in the Fourier series.

Iterative solvers [41, 42] are widely available to solve a general class of large linear systems that arise in many areas of science and engineering, with Krylov subspace methods being one of the most popular variants. Krylov subspace methods seek to develop a sequence of Krylov vectors where the lower dimensional subspace approximates the solution to a larger dimensional system of equations. Newton-Krylov methods (and Jacobian-free methods [43]) utilize Krylov subspace iterative solvers to approximate the inverse of the Jacobian matrix derived by the Newton-Raphson iteration scheme. Within path-following and continuation methods, the use of iterative solvers to approximate the solution within Newton-Raphson iterations provide opportunities to reduce the computational cost and memory usage compared to direct solvers [44]. Inexact Newton methods [45] provide a functional condition in which the approximate prediction and correction updates satisfactorily meets the required accuracy based on a numerical tolerance. There are several choices of iterative solvers [41, 42] whose performance depends on the specific problem and the properties of the system matrix. An important aspect of these solvers is the selection of a preconditioner to accelerate the number of iterations within the iterative solver [46].

Several studies in different fields of engineering have demonstrated the use of Newton-Krylov methods for the computation of periodic orbits. Rizzoli et al. [47, 48] proposed to use the inexact Newton method [45] combined with a preconditioned iterative solver [49] to compute the steady-state response of nonlinear microwave circuits under multitone excitation. The authors report that the block-diagonal Jacobian matrix provides an excellent preconditioner for a broad class of microwave circuit problems. Rhodes et al. [50, 51] also proposed a parallel and scalable MHB simulation method for nonlinear circuits analysis that leverages the circuit substructure form. Later, Dong and Li [52] developed a parallel MHB approach to solve both forced and autonomous circuits using hierarchical preconditioning methods to partition the linearized problem into smaller subdomains. A study by Soveiko et al. [53] evaluated the performance of the parallel solver in [54] for different computing architectures and discussed several practical considerations when implementing algorithms on certain computing hardware. Mehrotra et al. [55] developed a specialized direct solver for the Jacobian that arises from the MHB discretization to overcome the known challenges with iterative methods. A dual-primal finite element tearing and interconnecting (FETI-DP) domain decomposition method was deployed in [56] to directly divide the large-scale problem into smaller subdomains that can be solved in parallel. Han et al. [57] proposed a graph sparsification approach to generate the preconditioner for use in iterative solvers.

A Newton-Krylov method was proposed by Sánchez et al. [58] with continuation to calculate the periodic orbits of Navier-Stokes flows. Later, Net and Sánchez [59] proposed the use of iterative Newton-Krylov methods to track bifurcations of periodic orbits for large-scale, extended systems. The methods use the shooting and restarted generalized minimal residual method (GMRES) [49] and the authors applied the approach to thermal convection problems. A matrix-free method was proposed in [60], which also combines the shooting method with continuation to track the limit cycle oscillations of thermoacoustic systems as the system parameters change. Recently, the authors in [61] proposed an accelerated Krylov-subspace method with a modified Newton-Raphson scheme to perform continuation of periodic orbits of smooth and non-smooth mechanical systems. The method addresses the inversion of the Jacobian matrix of the Poincaré map which is known to be a large computational bottleneck. Sierra et al. [62] utilize the Fourier-Galerkin method to approximate the stable and unstable time-periodic motions and their sensitivities using adjoint methods and preconditioned Newton-Krylov methods. Other examples include the computation of flutter and limit cycle oscillations using time-spectral aeroelastic equations [63] and unsteady flows with oscillating shocks [64]. Blahos et al. [65] developed an approach based on parallel, sparse direct solvers to solve for nonlinear forced response of mechanical systems using sequential continuation.

In this paper, the authors propose a novel Newton-Krylov method within the MHB and pseudo-arclength continuation algorithm to improve the performance and efficiency for large-scale models. The developments throughout are applied to harmonically excited, non-conservative systems, i.e. NLFR curves, but the strategy can be generalized and applied to other time-periodic solutions such as NNMs or limit cycle oscillations. The inexact Newton scheme [45] provides a conditional statement in which the approximate prediction and correction updates are solved using an iterative solver strategy that recycles information from previous MHB solutions along the curve. The delayed frequency preconditioner (DFP) [66] recycles the preconditioner that is factorized at a prior solution point and is updated periodically depending on the performance of the iterative solver. The GCRO iterative solver with deflated restarting (GCRO-DR) [67] is a Krylov subspace recycling method that successively solves a sequence of linear systems that arise from the prediction and correction updates, and has found many applications in various areas of scientific computing, for example [68-73]. The iterative method uses harmonic Ritz vectors corresponding to the harmonic Ritz values with the smallest magnitude and uses these as the initial basis in the next iterative solve. The performance of the iterative solver using these two recycling strategies are investigated and compared to direct solvers used to obtain the necessary prediction and correction solutions to continue along the solution curve.

The paper is organized as follows. Section 2 reviews the MHB formulation and the resulting predictor-corrector algorithm when MHB is combined with pseudo-arclength continuation. Section 3 discusses the novel contributions to apply iterative solvers to the MHB algorithm. In particular, the GCRO-DR solver with DFP is adapted to the simulation framework to allow for the algorithm to recycle both the Krylov subspaces across a sequence of linear solves and the preconditioner factorized at a previous solution. Two numerical examples are provided in Section 4. The first model is a nonlinear electromechanical model of a mock pylon structure attached to a shaker and fixture with piecewise linear contact elements. The second example is a nonlinear beam assembly with bolt joints and frictional contact type nonlinearities that arise from a bolt preload simulation. These examples are used to demonstrate the speedup and performance of the iterative solver on moderately sized systems. Conclusions are provided in Section 5.

2. Computation of Periodic Orbits using Harmonic Balance

2.1 Frequency Domain Governing Equations

Starting with the non-autonomous, second order differential equations represented by the finite element method,

$$\mathbf{M}\ddot{\mathbf{x}} + \mathbf{C}\dot{\mathbf{x}} + \mathbf{K}\mathbf{x} + \mathbf{f}_{nl}(\mathbf{x}, \dot{\mathbf{x}}) = \mathbf{f}_{pre} + \mathbf{f}_{ext}(t) \tag{1}$$

the $n \times n$ matrices $\mathbf{M}$, $\mathbf{C}$, and $\mathbf{K}$ correspond to the mass, viscous damping and linear stiffness, respectively. The nonlinear restoring force, $\mathbf{f}_{nl}(\mathbf{x}, \dot{\mathbf{x}})$, is an $n \times 1$ vector, along with the vectors $\mathbf{f}_{pre}$ and $\mathbf{f}_{ext}(t)$, which are the time-independent preload force and time-varying harmonic force, respectively. The overdot represents the derivative with respect to time. The steady-state solution, i.e. assumed periodic motion, as well as the external excitation is approximated as a finite Fourier series as

$$\mathbf{x}(t) = \frac{\mathbf{c}_0^x}{\sqrt{2}} + \sum_{k=1}^{N_h}[\mathbf{s}_k^x \sin(k\omega t) + \mathbf{c}_k^x \cos(k\omega t)] \tag{2}$$

$$\mathbf{f}_{nl}(\mathbf{x}, \dot{\mathbf{x}}) = \frac{\mathbf{c}_0^{nl}}{\sqrt{2}} + \sum_{k=1}^{N_h}\left[\mathbf{s}_k^{nl} \sin(k\omega t) + \mathbf{c}_k^{nl} \cos(k\omega t)\right] \tag{3}$$

$$\mathbf{f}_{ext}(t) = \frac{\mathbf{c}_0^f}{\sqrt{2}} + \sum_{k=1}^{N_h}\left[\mathbf{s}_k^f \sin(k\omega t) + \mathbf{c}_k^f \cos(k\omega t)\right] \tag{4}$$

Here the fundamental harmonic frequency, ω, of the external forcing is assumed to be unknown, along with the unknown Fourier coefficients of the displacements and nonlinear restoring force, which are gathered into $(2N_h + 1)n \times 1$ vectors

$$\mathbf{z} = \left[(\mathbf{c}_0^x)^{\mathrm{T}} \quad (\mathbf{s}_1^x)^{\mathrm{T}} \quad (\mathbf{c}_1^x)^{\mathrm{T}} \quad \dots \quad (\mathbf{s}_{N_h}^x)^{\mathrm{T}} \quad (\mathbf{c}_{N_h}^x)^{\mathrm{T}}\right]^{\mathrm{T}} \tag{5}$$

$$\mathbf{b} = \left[(\mathbf{c}_0^{nl})^{\mathrm{T}} \quad (\mathbf{s}_1^{nl})^{\mathrm{T}} \quad (\mathbf{c}_1^{nl})^{\mathrm{T}} \quad \dots \quad (\mathbf{s}_{N_h}^{nl})^{\mathrm{T}} \quad (\mathbf{c}_{N_h}^{nl})^{\mathrm{T}}\right]^{\mathrm{T}} \tag{6}$$

The known, prescribed time-independent and time-dependent forcing terms are stored in the same sized vectors as

$$\mathbf{b}_{pre} = \left[(\sqrt{2}\mathbf{f}_{pre})^{\mathrm{T}} \quad \mathbf{0}^{\mathrm{T}} \quad \dots \quad \mathbf{0}^{\mathrm{T}}\right]^{\mathrm{T}} \tag{7}$$

$$\mathbf{b}_{ext} = \left[(\mathbf{c}_0^f)^{\mathrm{T}} \quad (\mathbf{s}_1^f)^{\mathrm{T}} \quad (\mathbf{c}_1^f)^{\mathrm{T}} \quad \dots \quad (\mathbf{s}_{N_h}^f)^{\mathrm{T}} \quad (\mathbf{c}_{N_h}^f)^{\mathrm{T}}\right]^{\mathrm{T}} \tag{8}$$

The continuous functions in Eqns. (2)-(4) are converted to discrete functions such that the sine and cosine functions are sampled over the fundamental period, leading to the discrete harmonic matrix,

$$\mathbf{Q}(\theta) = \left[\begin{bmatrix} 1/\sqrt{2} \\ 1/\sqrt{2} \\ \vdots \\ 1/\sqrt{2} \end{bmatrix} \begin{bmatrix} \sin(\theta_1) \\ \sin(\theta_2) \\ \vdots \\ \sin(\theta_N) \end{bmatrix} \begin{bmatrix} \cos(\theta_1) \\ \cos(\theta_2) \\ \vdots \\ \cos(\theta_N) \end{bmatrix} \dots \begin{bmatrix} \sin(N_h\theta_1) \\ \sin(N_h\theta_2) \\ \vdots \\ \sin(N_h\theta_N) \end{bmatrix} \begin{bmatrix} \cos(N_h\theta_1) \\ \cos(N_h\theta_2) \\ \vdots \\ \cos(N_h\theta_N) \end{bmatrix}\right] \tag{9}$$

Here $\theta_\mathrm{i} = \omega t_\mathrm{i}$ is discretely sampled between 0 and 2π-Δθ, where Δθ is the appropriate size of phase step [74]. The displacement, velocity and nonlinear restoring force are written in discrete form as

$$\tilde{\mathbf{x}} = (\mathbf{Q}(\theta) \otimes \mathbb{I}_n)\mathbf{z} = \mathbf{\Gamma}\mathbf{z} \tag{10}$$

$$\dot{\tilde{\mathbf{x}}} = \left(\dot{\mathbf{Q}}(\theta) \otimes \mathbb{I}_n\right)\mathbf{z} = \mathbf{\Gamma}_v\mathbf{z} \tag{11}$$

$$\tilde{\mathbf{f}}_{nl}(\mathbf{x}, \dot{\mathbf{x}}) = (\mathbf{Q}(\theta) \otimes \mathbb{I}_n)\mathbf{b} = \mathbf{\Gamma}\mathbf{b} \tag{12}$$

where $\otimes$ and $\mathbb{I}_n$ are the Kronecker tensor product and the identity matrix of size n, respectively. The linear operator $\mathbf{\Gamma}$ represents the discrete inverse Fourier transform to obtain the time-domain displacement and nonlinear restoring force, while $\mathbf{\Gamma}_v$ corresponds to the discrete inverse Fourier transform to obtain the time-domain velocity field. The latter is computed with the time derivative of the discrete harmonic matrix,

$$\dot{\mathbf{Q}}(\theta) = \left[\begin{bmatrix} 0 \\ 0 \\ \vdots \\ 0 \end{bmatrix} \begin{bmatrix} \omega\cos(\theta_1) \\ \omega\cos(\theta_2) \\ \vdots \\ \omega\cos(\theta_N) \end{bmatrix} \begin{bmatrix} -\omega\sin(\theta_1) \\ -\omega\sin(\theta_2) \\ \vdots \\ -\omega\sin(\theta_N) \end{bmatrix} \dots \begin{bmatrix} N_h\omega\cos(N_h\theta_1) \\ N_h\omega\cos(N_h\theta_2) \\ \vdots \\ N_h\omega\cos(N_h\theta_N) \end{bmatrix} \begin{bmatrix} -N_h\omega\sin(N_h\theta_1) \\ -N_h\omega\sin(N_h\theta_2) \\ \vdots \\ -N_h\omega\sin(N_h\theta_N) \end{bmatrix}\right] \tag{13}$$

The displacement, velocity and nonlinear restoring force in the time-domain are collected as vectors stacked at each discrete time sample,

$$\tilde{\mathbf{x}} = \left[(\mathbf{x}(\theta_1))^{\mathrm{T}} \quad (\mathbf{x}(\theta_2))^{\mathrm{T}} \quad \dots \quad (\mathbf{x}(\theta_N))^{\mathrm{T}}\right]^{\mathrm{T}} \tag{14}$$

$$\dot{\tilde{\mathbf{x}}} = \left[(\dot{\mathbf{x}}(\theta_1))^{\mathrm{T}} \quad (\dot{\mathbf{x}}(\theta_2))^{\mathrm{T}} \quad \dots \quad (\dot{\mathbf{x}}(\theta_N))^{\mathrm{T}}\right]^{\mathrm{T}} \tag{15}$$

$$\tilde{\mathbf{f}}_{nl}(\mathbf{x},\dot{\mathbf{x}}) = \left[\left(\mathbf{f}_{nl}\left(\mathbf{x}(\theta_1),\dot{\mathbf{x}}(\theta_1)\right)\right)^{\mathrm{T}} \quad \left(\mathbf{f}_{nl}\left(\mathbf{x}(\theta_2),\dot{\mathbf{x}}(\theta_2)\right)\right)^{\mathrm{T}} \quad \cdots \quad \left(\mathbf{f}_{nl}\left(\mathbf{x}(\theta_N),\dot{\mathbf{x}}(\theta_N)\right)\right)^{\mathrm{T}}\right]^{\mathrm{T}} \tag{16}$$

Additionally, the discrete Fourier transform is calculated using the pseudo-inverse, $(\,)^{\dagger}$, of Eqns. (10) and (12), leading to the form,

$$\mathbf{\Gamma}^{\dagger} = (\mathbf{Q}(\theta) \otimes \mathbb{I}_n)^{\dagger} = \left(\mathbf{Q}^{\dagger}(\theta) \otimes \mathbb{I}_n^{\dagger}\right) \tag{17}$$

The discrete Fourier transform can be obtained by performing the pseudo-inverse on the $N \times (2N_h + 1)$ matrix, $\mathbf{Q}(\theta)$, and only needs to be computed once with a sufficient sample rate for the harmonic order of the Fourier approximation. A similar operator is defined for the velocity as well.

The alternating time-frequency method [35] is used to approximate the Fourier coefficients in Eq. (6) from the time-domain nonlinear restoring force vector

$$\mathbf{b} = \mathbf{\Gamma}^{\dagger}\tilde{\mathbf{f}}_{nl} \tag{18}$$

In this way, the Fourier coefficients of the nonlinear force, $\mathbf{b}$, can be computed numerically by sampling the nonlinear restoring force in the time domain using Eq. (16) and transforming to the frequency domain using the discrete Fourier transform, $\mathbf{\Gamma}^{\dagger}$. This generally allows for the nonlinear functions to be implemented numerically in the time-domain and does not require an analytical derivation in the frequency domain. This formulation applies to all nonlinear constitutive elements of interest with an arbitrary number of harmonics in the Fourier series.

Following the derivation in [21, 36], a Fourier-Galerkin projection onto the orthogonal set of discrete periodic functions, $\mathbf{Q}(\theta)$, results in the MHB frequency domain governing equations,

$$\mathbf{r}(\mathbf{z},\omega) = \mathbf{A}(\omega)\mathbf{z} + \mathbf{b}(\mathbf{z}) - \mathbf{b}_{pre} - \mathbf{b}_{ext} \tag{19}$$

where $\mathbf{A}(\omega)$ is the linear portion of the dynamic stiffness matrix of dimension $(2N_h + 1)n \times (2N_h + 1)n$

$$\mathbf{A}(\omega) = \begin{bmatrix} \mathbf{K} & & & & \\ & \mathbf{K} - (\omega)^2\mathbf{M} & -\omega\mathbf{C} & & \\ & \omega\mathbf{C} & \mathbf{K} - (\omega)^2\mathbf{M} & & \\ & & & \ddots & \\ & & & \mathbf{K} - (N_h\omega)^2\mathbf{M} & -N_h\omega\mathbf{C} \\ & & & N_h\omega\mathbf{C} & \mathbf{K} - (N_h\omega)^2\mathbf{M} \end{bmatrix} \tag{20}$$

The roots of the residual function $\mathbf{r}(\mathbf{z},\omega)$ define the solutions to the nonlinear, algebraic system of equations that approximate the periodic solutions of Eq. (1). The pseudo-arclength continuation algorithm described in Section 2.2 requires the Jacobian of the residual with respect to $\mathbf{z}$ and ω. Following the methodology in Colaïtis et al. [21], the Jacobian matrix is analytically derived as,

$$\mathbf{r}_z(\mathbf{z},\omega) = \mathbf{A}(\omega) + \frac{\partial \mathbf{b}}{\partial \mathbf{z}} = \mathbf{A}(\omega) + \mathbf{\Gamma}^{\dagger}\frac{\partial \tilde{\mathbf{f}}_{nl}}{\partial \tilde{\mathbf{x}}}\mathbf{\Gamma} + \mathbf{\Gamma}^{\dagger}\frac{\partial \tilde{\mathbf{f}}_{nl}}{\partial \dot{\tilde{\mathbf{x}}}}\mathbf{\Gamma}_{\boldsymbol{v}} \tag{21}$$

$$\mathbf{r}_{\omega}(\mathbf{z},\omega) = \frac{\partial \mathbf{A}(\omega)}{\partial \omega}\mathbf{z} + \frac{\partial \mathbf{b}}{\partial \omega} = \frac{\partial \mathbf{A}(\omega)}{\partial \omega}\mathbf{z} + \mathbf{\Gamma}^{\dagger}\frac{\partial \tilde{\mathbf{f}}_{nl}}{\partial \dot{\tilde{\mathbf{x}}}}\frac{\partial \dot{\tilde{\mathbf{x}}}}{\partial \omega} \tag{22}$$

The time domain Jacobians $\frac{\partial \tilde{\mathbf{f}}_{nl}}{\partial \tilde{\mathbf{x}}}$ and $\frac{\partial \tilde{\mathbf{f}}_{nl}}{\partial \dot{\tilde{\mathbf{x}}}}$ can be calculated either analytically or numerically and transformed to the frequency domain using the discrete Fourier transform and its inverse. The Jacobians $\frac{\partial \mathbf{b}}{\partial \mathbf{z}}$ and $\frac{\partial \mathbf{b}}{\partial \omega}$ do not need to be derived explicitly and again can be applied to arbitrary forms of nonlinearity and harmonic order. The general form of time-domain Jacobians of the nonlinear restoring force in Eqns. (21) and (22) is a block matrix,

$$\frac{\partial \tilde{\mathbf{f}}_{nl}}{\partial \tilde{\mathbf{x}}} = \begin{bmatrix} \frac{\partial \mathbf{f}_{nl}(\theta_1)}{\partial \mathbf{x}(\theta_1)} & \frac{\partial \mathbf{f}_{nl}(\theta_1)}{\partial \mathbf{x}(\theta_2)} & \cdots & \frac{\partial \mathbf{f}_{nl}(\theta_1)}{\partial \mathbf{x}(\theta_N)} \\ \frac{\partial \mathbf{f}_{nl}(\theta_2)}{\partial \mathbf{x}(\theta_1)} & \frac{\partial \mathbf{f}_{nl}(\theta_2)}{\partial \mathbf{x}(\theta_2)} & \cdots & \frac{\partial \mathbf{f}_{nl}(\theta_2)}{\partial \mathbf{x}(\theta_N)} \\ \vdots & \vdots & \ddots & \vdots \\ \frac{\partial \mathbf{f}_{nl}(\theta_N)}{\partial \mathbf{x}(\theta_1)} & \frac{\partial \mathbf{f}_{nl}(\theta_N)}{\partial \mathbf{x}(\theta_2)} & \cdots & \frac{\partial \mathbf{f}_{nl}(\theta_N)}{\partial \mathbf{x}(\theta_N)} \end{bmatrix} \tag{23}$$

$$\frac{\partial \tilde{\mathbf{f}}_{nl}}{\partial \tilde{\mathbf{x}}} = \begin{bmatrix} \frac{\partial \mathbf{f}_{nl}(\theta_1)}{\partial \mathbf{x}(\theta_1)} & \frac{\partial \mathbf{f}_{nl}(\theta_1)}{\partial \dot{\mathbf{x}}(\theta_2)} & \cdots & \frac{\partial \mathbf{f}_{nl}(\theta_1)}{\partial \dot{\mathbf{x}}(\theta_N)} \\ \frac{\partial \mathbf{f}_{nl}(\theta_2)}{\partial \mathbf{x}(\theta_1)} & \frac{\partial \mathbf{f}_{nl}(\theta_2)}{\partial \dot{\mathbf{x}}(\theta_2)} & \cdots & \frac{\partial \mathbf{f}_{nl}(\theta_2)}{\partial \dot{\mathbf{x}}(\theta_N)} \\ \vdots & \vdots & \ddots & \vdots \\ \frac{\partial \mathbf{f}_{nl}(\theta_N)}{\partial \mathbf{x}(\theta_1)} & \frac{\partial \mathbf{f}_{nl}(\theta_N)}{\partial \dot{\mathbf{x}}(\theta_2)} & \cdots & \frac{\partial \mathbf{f}_{nl}(\theta_N)}{\partial \dot{\mathbf{x}}(\theta_N)} \end{bmatrix} \tag{24}$$

Note that for history *independent* nonlinearities, each off-diagonal matrix is zero and only the diagonal block matrices need to be computed.

2.2 Predictor-Corrector Algorithm

Pseudo-arclength continuation is combined with the MHB discretization in Eq. (19) to trace the NLFR curves of the system. This is done by appending an additional constraint equation to the MHB residual equation as,

$$\mathbf{R}(\mathbf{y}) = \begin{bmatrix} \mathbf{A}(\omega)\mathbf{z} + \mathbf{b}(\mathbf{z}) - \mathbf{b}_{pre} - \mathbf{b}_{ext} \\ \mathbf{V}^{\mathrm{T}}\left(\mathbf{y} - \mathbf{y}^{(\boldsymbol{k=1})}\right) \end{bmatrix} \tag{25}$$

The first row in the residual function, $\mathbf{R}(\mathbf{y})$, is the MHB residual in Eq. (19), while the second row is the additional constraint enforcing the solution, $\mathbf{y}$, to lie along a hyperplane tangent to a prediction vector, $\mathbf{V}$. The $(2N_h+1)n+1 \times 1$ vector $\mathbf{y} = [\mathbf{z}^{\mathrm{T}} \quad \omega]^{\mathrm{T}}$ is the collection of unknown variables and $\mathbf{y}^{(\boldsymbol{k=1})}$ is the initial predicted solution along the tangent of the curve. The following subsections discuss the implementation of the prediction and correction steps.

2.2.1 Prediction Step

Starting with a known solution along the branch, i.e. the j^{th} solution, $\mathbf{y}_{(j)}$, the prediction vector is computed tangent to the residual function, $\mathbf{r}\left(\mathbf{y}_{(j)}\right)$. Mathematically, the tangent vector, $\mathbf{V}_{(\boldsymbol{j})} = \left[\mathbf{V}_{\mathbf{z},(j)}^{\mathrm{T}} \quad V_{\omega,(j)}\right]^{\mathrm{T}}$, is solved as,

$$\begin{bmatrix} \mathbf{r}_{\mathbf{z}}\left(\mathbf{y}_{(j)}\right) & \mathbf{r}_{\omega}\left(\mathbf{y}_{(j)}\right) \\ \mathbf{V}_{\mathbf{z},(j-1)}^{\mathrm{T}} & V_{\omega,(j-1)} \end{bmatrix} \begin{bmatrix} \mathbf{V}_{\mathbf{z},(j)} \\ V_{\omega,(j)} \end{bmatrix} = \begin{bmatrix} \mathbf{0} \\ 1 \end{bmatrix} \tag{26}$$

The resulting predictor is normalized using the l^2 norm of the tangent vector such that $\left\|\mathbf{V}_{(j)}\right\| = 1$. An approximation to the next solution along the NLFR branch is obtained by taking a step along the direction of the prediction vector, whose magnitude, $h_{(j)}$, is automated based on the step size control algorithm presented in [75]; this is discussed further in Section 2.3. The magnitude controls the distance from the current solution, $\mathbf{y}_{(j)}$, based on the number of correction steps required to obtain a solution. The predicted solution along the curve is computed as,

$$\mathbf{z}^{(k=1)} = \mathbf{z}_{(j)} + h_{(j)}\mathbf{V}_{\mathbf{z},(j)} \tag{27}$$

$$\omega^{(k=1)} = \omega_{(j)} + h_{(j)}V_{\omega,(j)} \tag{28}$$

2.2.2 Correction Step

A Newton-Raphson correction scheme is derived by taking a Taylor series expansion of the residual, $\mathbf{R}(\mathbf{y})$, in Eq. (25) and truncating higher order terms. The initial guess for the correction scheme is provided by the predictions in Eqns. (27) and (28). This leads to the following linear system of equations,

$$\begin{bmatrix} \mathbf{r}_{\mathbf{z}}\left(\mathbf{y}^{(k)}\right) & \mathbf{r}_{\omega}\left(\mathbf{y}^{(k)}\right) \\ \mathbf{V}_{\mathbf{z},(\mathrm{j})}^{\mathrm{T}} & V_{\omega,(\mathrm{j})} \end{bmatrix} \begin{bmatrix} \Delta\mathbf{z}^{(k)} \\ \Delta\omega^{(k)} \end{bmatrix} = -\mathbf{R}\left(\mathbf{y}^{(k)}\right) \tag{29}$$

where $\mathbf{V}_{\mathbf{z},(\mathrm{j})}$ and $V_{\omega,(\mathrm{j})}$ are the prediction vectors computed at the j^{th} solution. The corrections are then used to update the variables

$$\mathbf{z}^{(k+1)} = \mathbf{z}^{(k)} + \Delta\mathbf{z}^{(k)} \tag{30}$$

$$\omega^{(k+1)} = \omega^{(k)} + \Delta\omega^{(k)} \tag{31}$$

The correction steps are repeated until the solution converges to satisfy the relative residual to a prescribed numerical tolerance,

$$\frac{\|\mathbf{R}(\mathbf{y}^{(k+1)})\|}{\|\mathbf{b}_{pre}+\mathbf{b}_{ext}\|} < \varepsilon_R \tag{32}$$

where $\|\ \|$ corresponds to the l^2 norm of a vector. Once this convergence tolerance is satisfied, the new solution along the curve is stored as

$$\mathbf{z}_{(j+1)} = \mathbf{z}^{(k+1)} \tag{33}$$

$$\omega_{(j+1)} = \omega^{(k+1)} \tag{34}$$

and the tangent vector, $\mathbf{V}_{(j+1)}$, is updated using Eq. (26) to predict the next solution along the curve.

2.3 Step Size Control and Branch Switching

The step size controller automatically adjusts the magnitude of the prediction step in Eqns. (27) and (28) based on the number of iterations to obtain a converged solution, $k_{(j)}$, and the optimal number of iterations specified by the user, k^*,

$$h_{(j+1)} = \left(\frac{k^*}{k_{(j)}}\right) h_{(j)} \tag{35}$$

where the sign of the step size is determined as

$$\text{sign}\left(h_{(j+1)}\right) = \text{sign}\left(h_{(j)}\mathbf{V}_{(j+1)}^{\mathrm{T}}\mathbf{V}_{(j)}\right) \tag{36}$$

The sign of the step size prevents the solution from turning back on itself. Within the continuation algorithm, a minimum and maximum step size is specified to provide reasonable bounds on $h_{(j+1)}$. Suboptimal, small step sizes lead to an excessive number of calculations to resolve the curve while excessively large steps lead to convergence issues and may not adequately resolve the important features of the forced response branch. As discussed in [12], the optimal number of iterations will depend on the solver used within the correction step. Depending on the solver, a less (more) accurate method will typically require a higher (lower) optimal number of iterations.

An additional check is performed prior to initiating the correction step from the predicted solution in Eqns. (27) and (28). The value of the residual at the predicted solution is enforced to be below a specified tolerance, such that

$$\frac{\|\mathbf{R}(\mathbf{y}^{(k=1)})\|}{\|\mathbf{b}_{pre}+\mathbf{b}_{ext}\|} < \varepsilon_V \tag{37}$$

If the residual is below this tolerance, then the correction step is initiated from the prediction. If not, then the step size is reduced successively until this condition is met. The purpose of this constraint is to prevent the prediction step from being too far from the solution curve and to avoid unnecessary correction iterations. This has been observed to occur for branches with sharp transitions, for example, with piecewise linear type nonlinear elements.

3. Iterative Solvers for Sparse Large-scale Systems

The focus of this research is to address the computational bottleneck associated with the MHB and pseudo-arclength continuation algorithm when solving large systems. During the continuation steps, a sequence of linear systems are solved, i.e. for the prediction vectors in Eq. (26), followed by a sequence of corrections in Eq. (29). The advantage of the scheme outlined in Section 2 is that the Jacobian matrices have the same form in the prediction and correction steps, each with linear systems of dimension $(2N_h+1)n \times (2N_h+1)n$. Direct solvers, such as those based on lower-upper (LU) or QR factorizations (see [76]), can efficiently and robustly calculate solutions to linear systems of small or moderate size. However, large-scale finite element models often possess many degrees of freedom in which case n is expected to be large. The resultant linear system further scales by the number of harmonics assumed in the finite Fourier series. Models relevant to computational structural dynamics require the solution to large-scale, linear systems for which direct solvers are inadequate due to memory limitations and poor scaling.

Krylov subspace-based iterative methods are a popular choice in a wide range of scientific applications to solve large-scale systems, and it is well understood that the speed and robustness of iterative solvers depends on many factors, including the selection of an appropriate preconditioner to accelerate convergence. In this work, a Newton-Krylov approach is developed to utilize a preconditioned iterative solver combined with an inexact Newton method to iteratively solve the sparse linear systems of the general form $\bar{\mathbf{A}}\bar{\mathbf{x}} = \bar{\mathbf{b}}$ in Eqns. (26) and (29). A schematic of the Jacobian matrix structure is shown in Fig. 1, which has a nonsymmetric, block-bordered form. The size of the matrix is dominated by the upper left quadrant, $\mathbf{r}_z(\mathbf{z}, \omega) = \mathbf{A}(\omega) + \frac{\partial \mathbf{b}}{\partial \mathbf{z}}$, which is a sparse matrix that is also nonsymmetric. In the absence of the nonlinear terms, $\frac{\partial \mathbf{b}}{\partial \mathbf{z}}$, the matrix $\mathbf{A}(\omega)$ is a block diagonal matrix since all the coupling terms across the harmonics of the Fourier series originate from the nonlinearity. The following subsections detail the preconditioned iterative solver utilized to repeatedly solve the sequence with this matrix form.

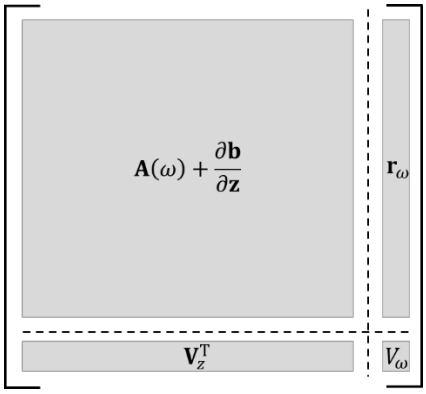

Figure 1. Schematic of the Jacobian $\mathbf{R}_\mathbf{y}$.

3.1 Inexact Newton Method

In general, the inexact Newton method [45] seeks to iteratively solve Eq. (25) by approximating the updates at each iteration, $\Delta\mathbf{y}^{(k)}$, by satisfying the inequality,

$$\left\|\mathbf{R}\left(\mathbf{y}^{(k)}\right) + \mathbf{R}_\mathbf{y}\left(\mathbf{y}^{(k)}\right)\Delta\mathbf{y}^{(k)}\right\| \leq \eta_k \left\|\mathbf{R}\left(\mathbf{y}^{(k)}\right)\right\| \tag{38}$$

The forcing term, $\eta_k \in [0,1)$, determines the required accuracy of the k^{th} correction $\Delta\mathbf{y}^{(k)}$. In the limit of the forcing term where $\eta_k = 0$, the method reduces to the Newton update. Any non-zero forcing term used is essentially a measure of the "inexactness" of the correction, allowing for the update to be approximated with a local linear model that reduces the norm of the residual function. The choice of forcing term can influence the efficiency and robustness of the method and several researchers have proposed various schemes for automating the forcing term [77, 78]. These methods lead to superlinear convergence, as opposed to quadratic convergence achieved with standard Newton-Raphson corrections. The inexact Newton method is a general framework to select the accuracy required for the correction at each iteration but does not specify how to obtain such approximation. The next subsection describes the GCRO-DR iterative solver to obtain the corrections, $\Delta\mathbf{y}^{(k)}$, in Eq. (38) as well as the predictions in Eq. (26) for an arbitrary level of accuracy dictated by the choice of forcing term.

3.2 GCRO with Deflated Restarting

The MHB with continuation algorithm relies on a repeated sequence of linear solves that consists of a single solve for a prediction step, followed by several solves within each correction iteration. A schematic of a single instance of the repeated process is shown in Fig. 2. In general, this results in a long sequence of linear systems where both the Jacobian matrix, $\mathbf{R}_\mathbf{y}$, and the right-hand side, generally written as the vector $\bar{\mathbf{b}}$ in Fig. 2, are changing from one iterative solve to the next. Furthermore, the next linear system in the sequence is dependent on the prior one, and thus the matrices and vectors cannot be known simultaneously, leading to a serial process. Krylov subspace-based iterative solvers rely on the subspace,

$$K_r(\mathbf{R_y}, \bar{\mathbf{b}}) = \text{span}(\bar{\mathbf{b}}, \mathbf{R_y}\bar{\mathbf{b}}, \mathbf{R_y^2}\bar{\mathbf{b}}, \dots, \mathbf{R_y^{r-1}}\bar{\mathbf{b}}) \tag{39}$$

where the subspace can be generated by the sequence of linear matrix-vector operations (assuming a zero initial guess). The approximate solution to the linear system is then sought within the *r*-dimensional subspace.

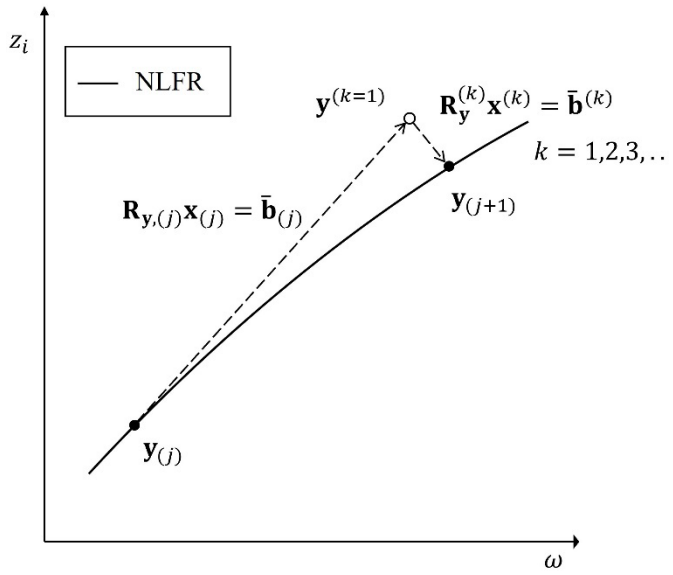

Figure 2. Sequence of linear solves within prediction and correction steps.

A straightforward implementation of iterative solvers generates a Krylov subspace that is, in theory, generated for each linear system solved in the sequence. This can be accomplished by approximately solving the linear system with, for example, the preconditioned GMRES solver originally developed by Saad et al. [49]. This method is known to work well for large, sparse, nonsymmetric linear systems such as the Jacobian matrix of interest here. As outlined in the next subsection, the preconditioner for the sequence of linear systems can be reused, or recycled, across the sequence of linear solves and refactorized periodically based on the performance of the algorithm. Additionally, assuming the linear system does not change significantly from one solve to the next, a portion of the Krylov subspace generated by the previous linear system can be recycled and reused for the next linear system. This is referred to as Krylov subspace recycling and can further speed up the convergence by reducing the number of iterations. The review paper by Soodhalter et al. [79] provides an overview of subspace recycling methods.

GCRO-DR [67] is used to successively solve the sequence of linear systems that arise in Fig. 2. The method utilizes $\tilde{k}$ harmonic Ritz vectors corresponding to the harmonic Ritz values with the smallest magnitude. This subspace is computed from the previous system of equations to provide an initial subspace for the iterative solver of the next system. The optimal solution is determined based on the initial subspace followed by a successive generation of additional Krylov vectors that augment the ones formed by the harmonic Ritz vectors. This process is repeated for each successive linear system in the sequence of solves associated with the MHB code. The interested reader is referred to the details in [67], particularly the pseudo code the authors provide in the appendix. In the results section that follows, the method will be described as GCRO-DR($\tilde{m}, \tilde{k}$), where $\tilde{m}$ is the maximum size of the subspace generated by the iterative solver, and $\tilde{k}$ is the number of eigenvectors to utilize in the subspace recycling between linear systems. These values must be selected based on the expected size of the subspace needed to solve the linear system; one approach to achieve this is to solve the system with arbitrarily high values first to approximate the number of iterations/vectors generated for each solution.

3.3 Delayed Frequency Preconditioner

An ideal preconditioner for iterative solvers of sparse linear systems is one that is inexpensive to compute and reduces the spectral condition of the general system matrix $\bar{\mathbf{A}}$. Furthermore, a preconditioner that can be reused or

recycled is advantageous since the factorization of the preconditioner can be costly, especially if it is recomputed for every correction and prediction step. In this study, the concept of the DFP from [66] is used to recycle the factorization of the matrix, $\mathbf{R_y}$, and the preconditioner is reused for several prediction/correction cycles along the NLFR branch in Fig. 2. Note that the recycled harmonic Ritz vectors in GCRO-DR are discarded at each refactorization. Within this framework, any type of preconditioner can be deployed to represent the approximate inverse of the Jacobian, $\mathbf{R_y}^{-1}$. As discussed in [66], the efficiency of the preconditioner often deteriorates as the solution moves away from the point on the curve at which the factorization occurred. Therefore, the preconditioner is periodically updated and re-factorized depending on the logical conditions requiring an update.

The approach in [66] required that the preconditioner be re-computed if the number of solver iterations exceed a fixed value. This works reasonably well for linear systems and favorable speedups are observed with this approach. In the current research, which applies DFP to nonlinear systems, it has been observed that the performance of the preconditioner within the GCRO-DR solver depends on the strength of the nonlinearity, which changes along the solution branch. Using a pre-determined and fixed value for the number of iterations that require a refactorization presents a challenge since this performance metric is problem dependent, potentially leading to suboptimal conditions that cause the preconditioner to be updated too frequently. To circumvent this, a new algorithm is proposed to adaptively update the preconditioner and is described in the pseudo code in Table 1.

The logical conditions proposed to update the preconditioner in Table 1 is an adaptation of the approach in [66] and is based on the average number of iterations within a single predictor-corrector step. The threshold for the number of iterations changes along the solution path and is updated throughout the simulation. The scale factor, $\zeta > 1$, dictates the threshold as to when the preconditioner should be recomputed for the previously determined number of iterations at the last re-factorization. The larger the value of ζ means that the preconditioner will be updated less often. Higher values of ζ should be used in cases when the cost of the factorization is high, and vice versa. This heuristic approach for selecting an optimal scaling factor, ζ, is also problem dependent based on the cost associated with the factorization, but allows for an adaptive method within the MHB algorithm so that the method adapts to the solution along the branch (e.g. in strongly nonlinear versus nearly linear regions).

Table 1. Algorithm for updating preconditioner

1: Perform preconditioner factorization of $\mathbf{R_y}$ using initial guess; define ζ
2: Perform initial correction and prediction, record total number of solver iterations as $n_{iter,(1)}$ within the predictor and corrector step.
3: $n_{exceed} = \zeta\left(\frac{n_{iter,(1)}}{k_{(1)}+1}\right)$ where $k_{(1)}$ is the number of correction steps; update = 0
4: **for** j = 2 to number of solution points
5: Compute corrections with preconditioned GCRO-DR and check convergence per Eqns. (29) and (32)
6: If converged, calculate the prediction step per Eq. (26) using preconditioned GCRO-DR
7: Record total number of solver iterations needed to perform correction and prediction in lines 5 and 6 as $n_{iter,(j)}$
8: **if** update = 1; **then** $n_{exceed} = \zeta\left(\frac{n_{iter,(j)}}{k_{(j)}+1}\right)$; update = 0; **end**
8: **if** $\left(\frac{n_{iter,(j)}}{k_{(j)}+1}\right) > n_{exceed}$; **then** update preconditioner factorization and discard recycled subspace in GCRO-DR; update = 1; **end**
9: **end**

In this study, four different preconditioning strategies are used within the DFP algorithm in Table 1. Each method creates sparse lower and upper triangular matrices, generically denoted **L** and **U**, which form the matrices of the preconditioner. The book by Saad [42] provides excellent overview regarding the solution of sparse linear systems using iterative methods. Chapter 10 covers a variety of preconditioning techniques, including incomplete

lower-upper (iLU) factorization. Variations of the iLU factorization include zero fill-in method, denoted iLU(0) or iLU(p) which account for some fill-in. Within MATLAB, there is an option to perform the Crout version of the iLU factorization, which is denoted as iLUC. In addition to the options available for preconditioning, it can be advantageous to reorder the Jacobian matrix prior to factorization to produce triangular matrices with more sparsity. This has been observed to improve both the cost of the iLU factorization as well as the cost of evaluating the preconditioner within each iterative solve. The results in the next section utilize the LU factorization, the iLU(0) and iLUC variants for incomplete factorization, as well as an iLUC factorization on each block-diagonal (BD-iLUC) matrix shown in the upper left quadrant in Fig. 1. For the LU and iLU factorizations on the full Jacobian matrix, the matrix is sorted using the nested dissection permutation [80], which is a multilevel graph partitioning algorithm. The BD-iLUC preconditioner was calculated in serial using a single processor but could readily extended to multi-core parallel processing.

4. Numerical Results

4.1 Mock Pylon with Electromechanical Shaker

The first numerical example is a mock pylon structure attached to a test fixture, as shown in Fig. 3. A 5-DOF model of an electromechanical shaker is coupled to the fixture-pylon model to capture the dynamics of the shaker-structure interaction. The input into the system is modeled as a sinusoidal voltage source supplied from a data acquisition system with a fixed voltage amplitude of 0.025 V. The source of nonlinearity in the model comes from the unilateral contact defined at the small gap between the thin strip and the two upper blocks of the pylon. A total of 90 node pairs are defined and the unilateral contact elements are power-function-based nonlinear penalty springs [81, 82] with $m = 2$ being the exponent and $k_n = 3.5 \cdot 10^{10}\ N/m$ being the penalty stiffness. The finite element model of the fixture and pylon were reduced to a Hurty-Craig/Bampton (HCB) model [83, 84] with a total of 50 fixed-interface modes, and 189 boundary DOF. When coupled to the shaker, the total size of the nonlinear reduced order model is 243 DOF. Within the 189 boundary DOF set, 180 DOF were selected for the z-displacement of the contact nodes, and the remaining 9 correspond to the x, y, and z displacement of the fixture attachment node and two accelerometer nodes on the swinging mass. The material list and properties of the pylon and fixture are listed in Table 2, while the parameters of the electrodynamical shaker match those reported in [85].

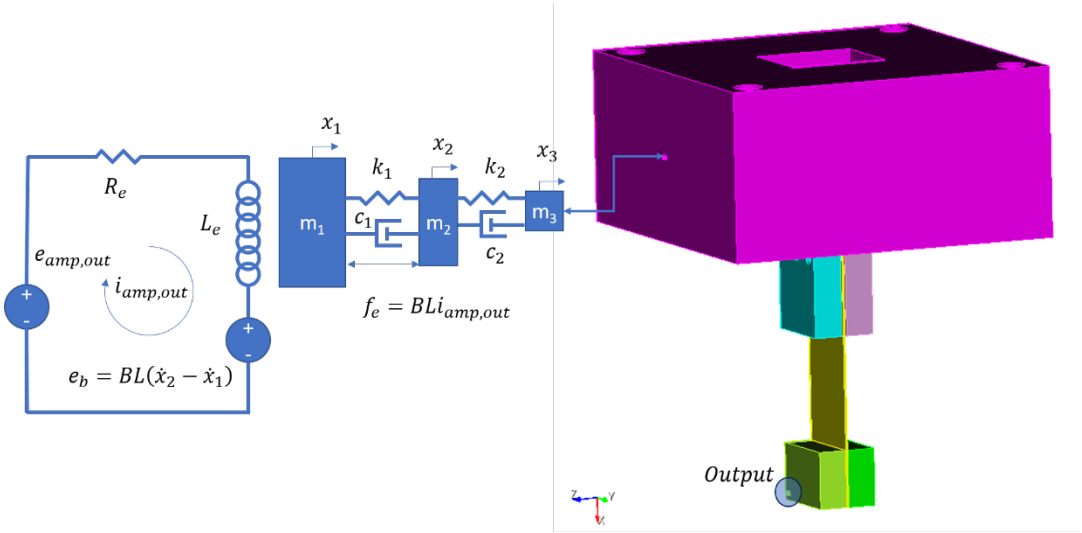

Figure 3. Schematic of mock pylon component attached to fixture block and electromechanical shaker.

Table 2. Isotropic linear elastic material properties

Material	Young's Modulus	Poisson's Ratio	Density	Assigned Blocks
6061-T6	68.9 GPa	0.30	2885 kg/m^3	Thin strip, mounting blocks, fixture

304 Stainless Steel	207 GPa	0.29	7790 kg/m^3	Swinging mass, washers

The NLFR curves for the shaker-fixture-pylon system are computed around the first resonance of the pylon, which is a bending mode with a linearized frequency of 8.8 Hz. For reference, the following parameters have been fixed for the MHB and continuation algorithm. The accepted relative tolerance of the residual from the corrections in Eq. (32) is $\varepsilon_R = 1 \cdot 10^{-6}$ while the residual tolerance for the acceptable predicted solution is $\varepsilon_V = 10$ in Eq. (37). A total of 2048 time steps are used in the AFT method to sample the nonlinear force vector and the derivatives, and a total of 400 solution points are calculated along the NLFR branch. For the step size controller, the optimal number of iterations in Eq. (35) are $k^* = 4$ while the maximum number of iterations is 8. For the iterative solvers, the relative tolerance of 10^{-6} is used to approximate the correction updates, while 10^{-8} is used for the predictions.

The NLFR curves are calculated around the first pylon resonance and are shown in Fig. 4. At low response amplitudes, the contact nonlinearity does not engage between the thin strip and upper blocks since the motion amplitude is not large enough to close the small gap that exists in the model. At high enough responses, however, the contact engages and thus there is a hardening effect on the resonance of the fundamental pylon mode. The plots in Fig. 4 show the resulting responses computed using MHB of different orders of Fourier series approximation. In these results, the direct solver in MATLAB used the *mldivide* function, which calls the CHOLMOD package. The solver is a supernodal Cholesky factorization method for sparse symmetric and nonsymmetric matrices [86]. Here the notation in the legend, i.e. k = 1: N_h, corresponds to the number of harmonics of the approximate Fourier solution in Eqns. (2)-(4). Increasing the number of harmonics scales the size of the linear system solved within the prediction and correction steps by $2N_h n$, where in this case the model size is n = 243. For example, when approximating the response with 80 harmonics, the coefficient matrix of the linear system is $38{,}880 \times 38{,}880$. The results in Fig. 4a show the resulting peak acceleration predicted at the output location in Fig. 3, while Fig. 4b shows the peak load cell force, which represents the reaction force between the fixture and load cell mass in the coupled shaker-structure model. Visually the results appear to converge with a harmonic order up to $N_h = 80$. These three simulation cases and their performance serve as references when comparing the computational cost of the direct solver to the iterative solvers.

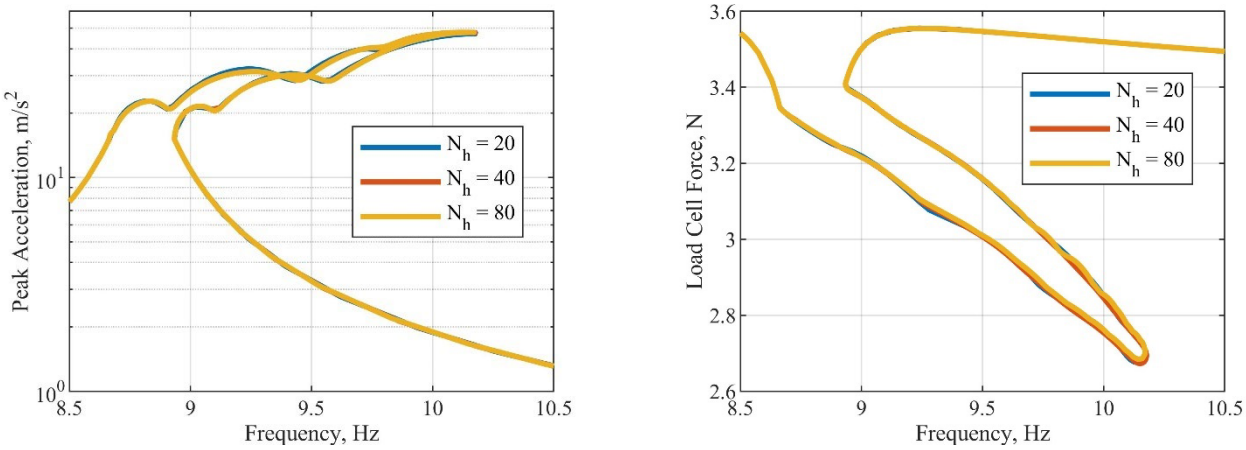

(a) (b)

Figure 4. NLFR of the first resonance using the direct solver with increasing number of harmonics showing the (a) peak acceleration and (b) peak load cell force versus excitation frequency.

The solutions from Fig. 4 were recomputed using the iterative solver outlined in Section 3. The GCRO-DR($\tilde{m}, \tilde{k}$) method is utilized with different values for $\tilde{m}$ and $\tilde{k}$. When these two parameters are set to arbitrarily large values (i.e. greater than the number of iterations needed to approximately solve the linear systems), the solver becomes the non-restarted version of GMRES. At lower values of $\tilde{m}$ and $\tilde{k}$, the solver then recycles the Krylov subspace

and can restart depending on the value of $\tilde{m}$. In this way, two iterative solvers are compared, namely non-restarted GMRES and GCRO-DR. In addition to the two iterative solvers, four types of preconditioners are utilized, namely the zero fill-in iLU(0) and the Crout version iLUC, as well as the LU and BD-iLUC factorizations. All of these preconditioners are readily integrated into the DFP algorithm in Table 1.

Prior to comparing the performance of the different solvers and preconditioners, a series of simulations were performed using non-restarted GMRES with both iLU preconditioners (iLU(0) and iLUC) to evaluate the computational cost with respect to the heuristic scale factor, ζ, in Table 1. This value dictates how frequently the preconditioner should be updated. The computational cost for the two preconditioners used with the non-restarted GMRES algorithm are evaluated in Fig. 5 for a range of ζ between 1.5 and 5 with a fixed number of harmonics, $N_h = 40$. The total solver cost for iterative solvers involved both the cost of the iterative solver plus the added cost to initialize and recalculate the preconditioner along the solution branch. Based on the results with the iLUC preconditioner, there is a trend where the cost of the solver increases with increasing ζ but the cost of the preconditioner decreases since it is recomputed less frequently. For $\zeta > 3$, these costs balance each other such that total cost for the iLUC preconditioner appears to be constant, at least in the range of values shown. For the zero fill-in iLU(0) preconditioner, the total cost coincides with the solver cost, since the cost of the preconditioner is relatively negligible. Because of this, the total cost is driven by the performance of the solver, which appears to be constant for $\zeta > 4$.

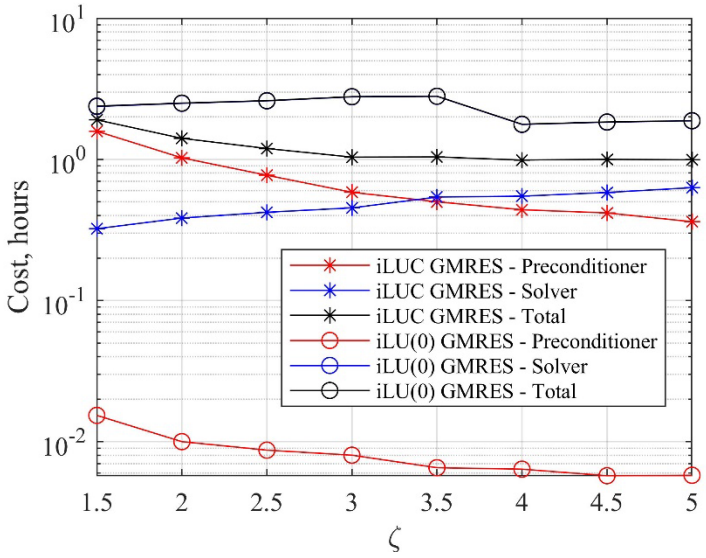

Figure 5. Performance of scale factors in Table 1 for GMRES with $N_h = 40$.

The results in Fig. 6 show the breakdown of the solver costs as a function of the number of harmonics in the MHB Fourier approximation for both non-restarted GMRES and GCRO-DR with subspace recycling. All preconditioner and iterative solver combinations provide favorable performance speedups relative to the direct solver. For the direct solver, the computational cost is only associated with the linear solves within the prediction and correction steps whereas the iterative solver accounts for the solver cost in addition to the cost to factorize the preconditioner. With the non-restarted GMRES solver, the LU, iLUC and iLU(0) preconditioners used a scale factor of $\zeta = 4$, while BD-iLUC used $\zeta = 2$. With GCRO-DR, the LU and iLUC preconditioners used a scale factor of $\zeta = 4$, while iLU(0) and BD-iLUC used $\zeta = 2$. Table 3 reports all the speedups achieved for each order of the Fourier series approximation, which is defined as the ratio of the direct solver cost over the indirect solver cost.

The LU and iLUC preconditioners are considered the more accurate representations of the system matrix, and thus have higher computational cost associated with their computation. The LU factorization provides only about 2x speedup for both non-restarted GMRES and GCRO-DR, compared to up to 9x speedup for the iLUC preconditioner. When using these two preconditioners with the GCRO-DR solver with $\tilde{k} = 5$ and $\tilde{m} = 1000$,

there is no favorable computational gain with the use of Krylov subspace recycling. The other two preconditioners, namely iLU(0) and BD-iLUC, are considered less accurate representations of the sytem matrix, and thus are less costly to compute compared to the LU and iLUC counterparts. Note that the cost of these preconditioners are negligible and thus the only visible cost in the bar plots correspond to the solver cost. The non-restarted GMRES solver with iLU(0) and BD-iLUC showed speedups ranging from 2x to 5x. When leveraging the subspace recycling with GCRO-DR, there was a significant improvement in the computational performance, resulting in speedups ranging from 4x to 7x. The iLU(0) and BD-iLUC preconditioners used subspace sizes of $\tilde{k} = 75$ and $\tilde{m} = 150$, except for the case when $N_h = 80$ with iLU(0), in which $\tilde{k} = 50$ and $\tilde{m} = 200$. (The latter settings are adjusted since the solver stalls with the other settings.) These results highlight the performance variability with iterative solvers and their dependence on preconditioning.

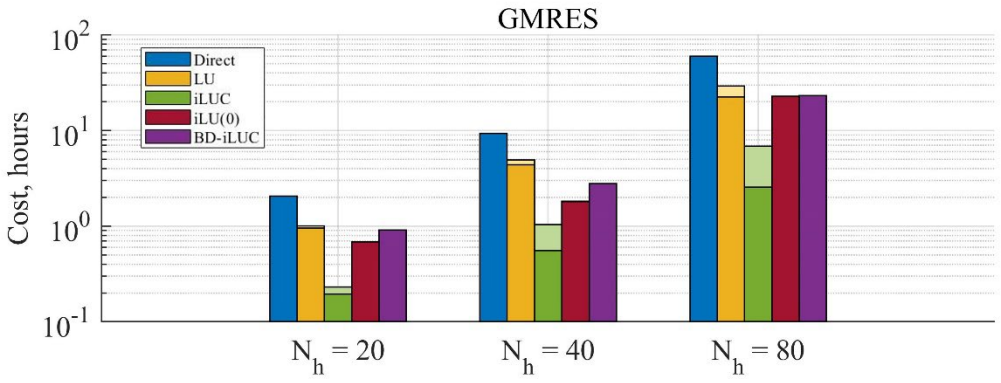

(a)

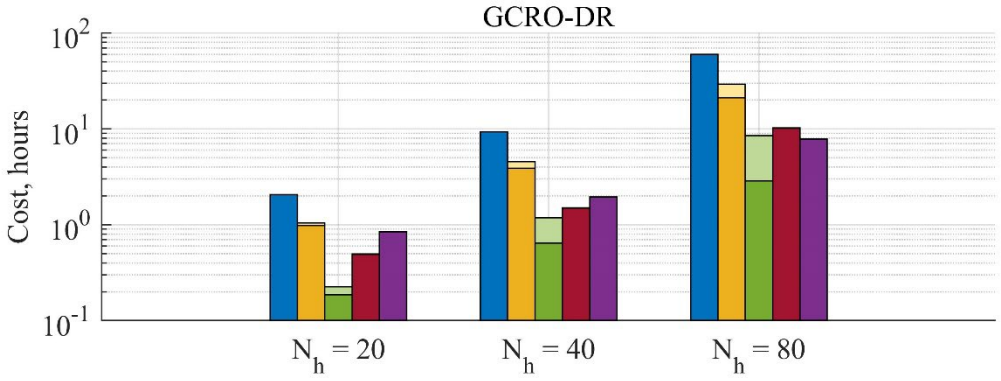

(b)

Figure 6. Solver cost comparison for (a) non-restarted GMRES and (b) GCRO-DR with different preconditioners applied to the pylon. Iterative solver costs decomposed into solver cost (lower bar) and preconditioner cost (upper bar).

Table 3. Speedups for each solver and preconditioner.

	GMRES			
	LU	iLUC	iLU(0)	BD-iLUC
$N_h = 20$	2.06	8.93	3.01	2.26
$N_h = 40$	1.90	9.03	5.15	3.35
$N_h = 80$	2.05	8.75	2.61	2.58
	GCRO-DR			
$N_h = 20$	1.98	9.16	4.16	2.44

$N_h = 40$	2.05	7.94	6.21	4.79
$N_h = 80$	2.05	7.02	5.86	7.57

The performance of the solvers in Fig. 6 are further evaluated by comparing the total number of iterations for all the preconditioners and solvers, as listed in Table 4. The LU and iLUC preconditioners show that each solution required between 20,000 to 40,000 total iterations for both the GMRES and GCRO-DR solver. In these cases, the use of subspace recycling did not accelerate the convergence of the solver significantly, thus explaining the lack of computational performance gains observed in Table 3. An additional cost is embedded in the solver to calculate the harmonic Ritz vectors and orthogonalize these with each linear system, so these added costs slightly increase the total solver cost. The subspace recycling does not provide any apparent advantage in the case of the LU and iLUC preconditioning. Another notable observation is the similarity of the number of iterations between LU and iLUC, but the iLUC preconditioner significantly outperformed the LU factorization. This is due to the sparsity of the incomplete factorization and the reduced number of computations associated with the matrix-vector products. For the case of iLU(0) and BD-iLUC with non-restarted GMRES, the solver iterations that were an order of magnitude higher than the LU and iLUC versions. The use of subspace recycling showed a significant improvement in the solver convergence by significantly reducing the number of iterations when using GCRO-DR. This performance improvement provides an explanation to the computational speedups reported in Table 3. These results highlight that the accelerated convergence properties of subspace recycling are best achieved with less accurate preconditioners, which often are less costly to compute. For cases in which the preconditioner is highly accurate (e.g. LU factorization), the subspace recycling does not provide favorable performance improvement.

Table 4. Total number of iterations for each solver and preconditioner.

	GMRES			
	LU	iLUC	iLU(0)	BD-iLUC
$N_h = 20$	19,498	23,795	126,261	115,093
$N_h = 40$	28,412	23,097	163,278	170,019
$N_h = 80$	40,182	37,198	750,248	493,455
	GCRO-DR			
$N_h = 20$	19,691	19,492	47,840	54,511
$N_h = 40$	23,151	23,319	76,313	59,482
$N_h = 80$	34,748	33,676	362,368	133,701

4.2 C-Beam with Small Deformation Frictional Contact

The next exemplar demonstrates the method on a reduced order model of the C-beam assembly shown schematically in Fig. 7. A finite element mesh of the beam is generated using CUBIT [87] followed by a HCB reduction [83, 84] using the Sierra/SD finite element software [88]. The finite element model assumes that the beams are made of steel with a Young's modulus of 200 GPa, density of 7,800 kg/m^3, and Poisson's ratio of 0.285. The beam assembly is suspended by soft suspension springs with a stiffness of $k_{suspension}$ = 3,065 N/m applied in the three displacement directions to mimic free-free boundary conditions. A total of 25 fixed-interface modes are generated for the HCB reduction basis, along with a total of 3,675 boundary DOF. The latter DOF set corresponds to a total of 1,220 total nodes defined within the contact surfaces of the beam interfaces, each with three translational DOF in x-, y- and z-directions. There are four nodes that correspond to the ends of the beam elements to apply the external preload, and a single node at the mid-point of one of the beams at which the harmonic time-varying force is applied.

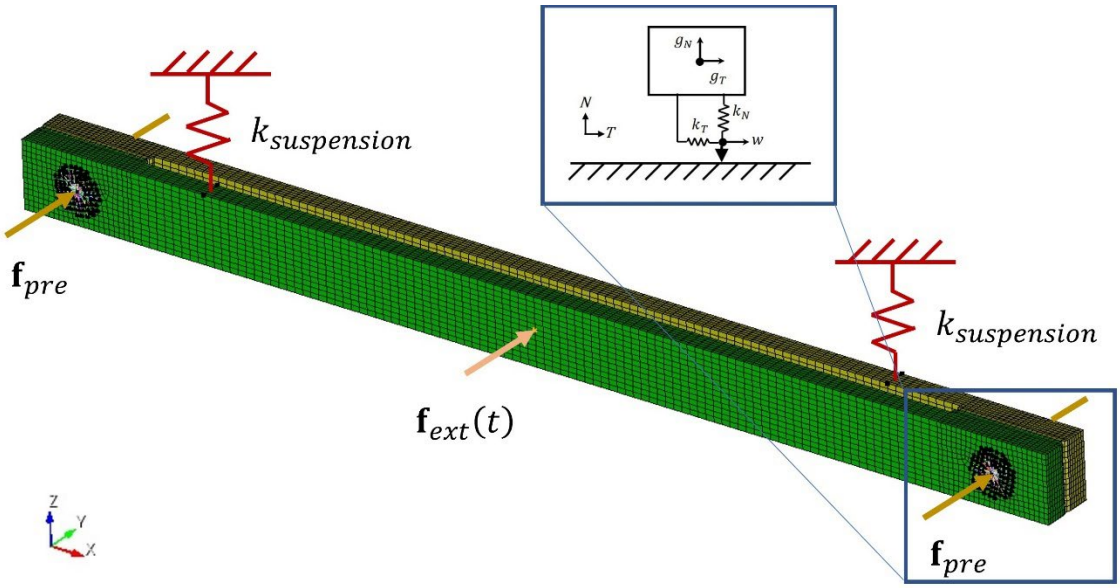

Figure 7. Schematic of C-beam assembly with node-to-node Jenkin's elements at contact node pairs.

A total of 610 Jenkins elements [89] are added to the a priori defined node pairs in the reduced HCB model prior to the application of the bolt preload forces. Each element has a normal penalty stiffness of $k_N = 1{\cdot}10^9$ N/m, tangential stiffness of $k_T = 5{\cdot}10^8$ N/m, and static coefficient of friction of $\mu = 0.6$. Prior to the MHB simulations, a bolt preload of 58.9 kN is applied to the model to capture the preload equilibrium state, which is needed to initialize the NLFR solution. The NLFR curves for the C-beam are computed around the second elastic mode corresponding to an in-phase bending mode of the two beams, which activates a softening nonlinearity due to the tangential slip regions developed through the shear stresses. The natural frequency of the system linearized about the preloaded equilibrium is 346.9 Hz. The following parameters are fixed for the MHB and continuation algorithm. The accepted relative tolerance of the residual from the corrections in Eq. (32) is $\varepsilon_R = 1 \cdot 10^{-6}$ while the residual tolerance for the acceptable predicted solution is $\varepsilon_V = 0.1$ in Eq. (37). A total of 2048 time steps are used in the AFT scheme to sample the nonlinear force vector, and a total of 150 solution points are calculated along the NLFR branch. For the step size controller, the optimal number of iterations in Eq. (35) are $k^* = 3$ while the maximum number of iterations was 6. For the iterative solvers, the relative tolerance of 10^{-6} is used to approximate the correction updates, while 10^{-8} is used for the predictions.

The plots in Fig. 8 show the NLFR solution with the direct solver around the second resonance, showing the peak acceleration at the drive-point location in the y-direction. The solution is computed for harmonics up to fifth order, which visually converge near the resonance peak. These solution cases serve as the reference solution when comparing the performance to the iterative solvers. The model size is $n = 3{,}712$, so when approximating the response with $N_h = 5$ harmonics, the coefficient matrix of the linear system is $40{,}832 \times 40{,}832$. Note that this system scales as $(2N_h + 1)n$ since an additional DC term is needed to capture the preload equilibrium state of the model. In these results, the direct solver in MATLAB used the *mldivide* function, which calls the UMFPACK package. The solver is a multifrontal LU factorization method for nonsymmetric sparse linear systems [90].

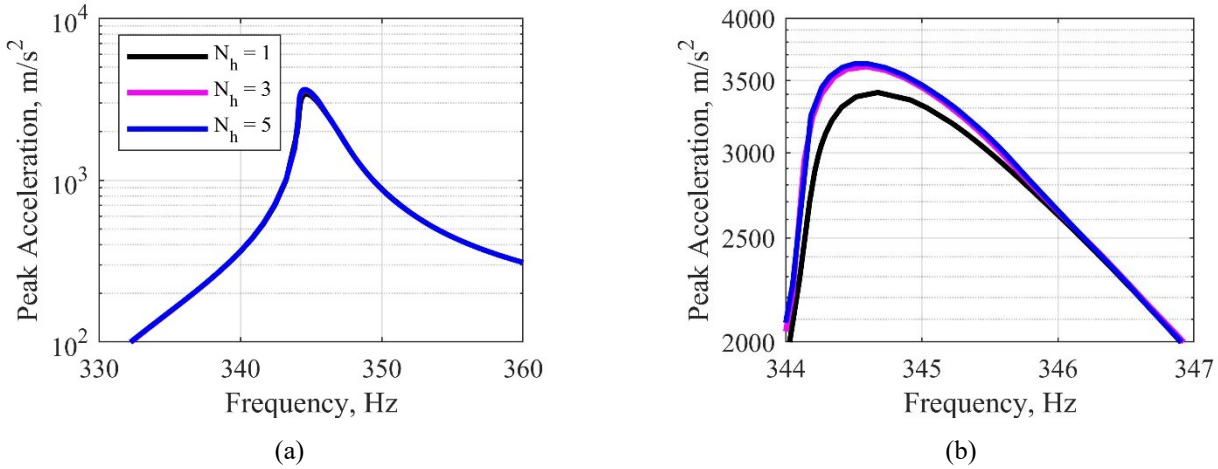

Figure 8. (a) NLFR near the second elastic mode with increasing number of harmonics; (b) zoomed in near the resonance peak.

The plots in Fig. 9 show the computational cost comparison between the two iterative solvers and the four preconditioners, which are again compared against the costs of the direct solver. Table 5 lists a summary of the speedups achieved with each solution and method. For these simulations, the scaling factor of $\zeta = 2$ is used for iLU(0) and BD-iLUC and $\zeta = 4$ for LU and iLUC. For the iLU(0) preconditioner with GCRO-DR, the following settings are used respectively for $N_h = 1,3,5$: $\tilde{m} = 100, 200, 400$ and $\tilde{k} = 50, 100, 200$. The case of LU, iLUC, and BD-iLUC with GCRO-DR uses $\tilde{m} = 40$ and $\tilde{k} = 20$ for all harmonics. Contrary to the previous pylon model, the non-restarted GMRES with LU and iLU(0) performs worse than the direct solver, reporting speedups < 1, highlighting the fact that iterative solvers do not necessarily outperform direct solvers. When using iLU(0) with the GCRO-DR subspace recycling, there is a significant improvement in the performance and results in favorable speedups compared to the direct solver. Contrary to this, the use of subspace recycling (GCRO-DR) with the other preconditioners (LU, iLUC, BD-iLUC) deteriorates the performance of the iterative solver compared to using them with the non-restarted GMRES solver.

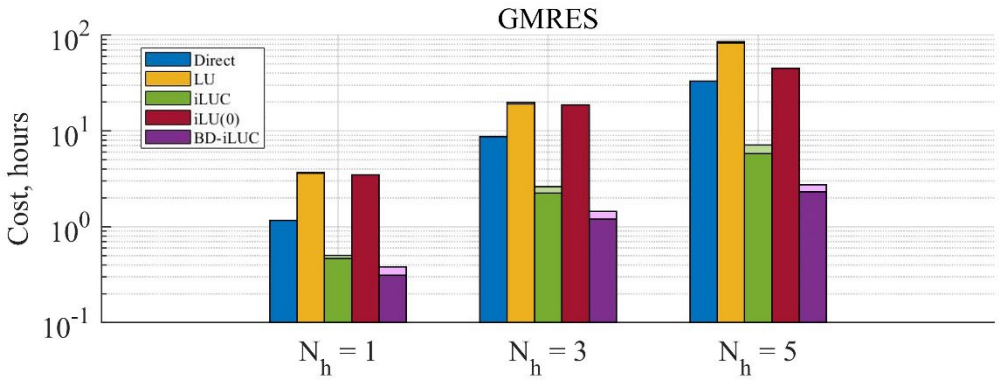

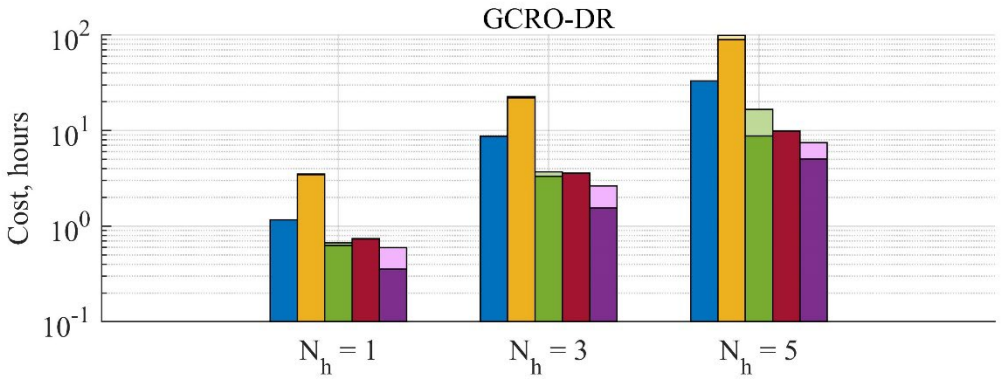

(b)

Figure 9. Solver cost comparison for (a) non-restarted GMRES and (b) GCRO-DR with different preconditioners applied to the C-Beam. Iterative solver costs decomposed into solver cost (lower bar) and preconditioner cost (upper bar).

Table 5. Speedups for each solver and preconditioner.

	GMRES			
	LU	iLUC	iLU(0)	BD-iLUC
$N_h = 1$	0.32	2.31	0.33	3.05
$N_h = 3$	0.44	3.33	0.47	6.04
$N_h = 5$	0.39	4.63	0.73	12.05
	GCRO-DR			
$N_h = 1$	0.33	1.73	1.57	1.94
$N_h = 3$	0.38	2.35	2.42	3.30
$N_h = 5$	0.33	1.99	3.34	4.43

The computation costs and relative speedups are further analyzed by investigating the total number of iterations for the NLFR branch as shown in Table 6. The LU and iLUC preconditioners show that each solution required between 10,000 to 20,000 total iterations for both the GMRES and GCRO-DR solver. The BD-iLUC preconditioner outperformed these two preconditioners by reporting approximately 5,000 to 13,000 iterations for the two solvers. It can be observed from Table 6 that the LU, iLUC, and BD-iLUC preconditioners with GCRO-DR subspace recycling did not accelerate the convergence of the solver significantly, thus explaining the decrease in computational performance listed in Table 5. With the iLU(0) preconditioner with non-restarted GMRES, the solver iterations were again an order of magnitude higher than the LU and iLUC versions, along with BD-iLUC for this example. The use of subspace recycling showed a significant improvement in the solver convergence by significantly reducing the number of iterations when using iLU(0) GCRO-DR, reducing it to a range between 20,000 to 60,000 iterations. Again, this reduction in iterations provides evidence for the computational speedups with subspace recycling reported in Table 5. As observed with the pylon model, the subspace recycling method works best with less accurate preconditioners. In the C-Beam example, the BD-iLUC preconditioner outperformed the other variants, contrary to the pylon model. The block-diagonal preconditioner neglects the off-diagonal block matrices, which are the coupling terms between the harmonics due to the nonlinearity. This preconditioner is more accurate for weaker nonlinearity types compared to stronger nonlinearities where these couplings are more dominant in the Jacobian matrix.

Table 6. Total number of iterations for each solver and preconditioner.

	GMRES			
	LU	iLUC	iLU(0)	BD-iLUC
$N_h = 1$	11,745	11,716	151,535	5,604
$N_h = 3$	14,250	14,620	305,963	7,910
$N_h = 5$	17,841	18,175	464,212	9,381
	GCRO-DR			
$N_h = 1$	9,753	9,536	19,634	4,527
$N_h = 3$	14,380	14,907	33,360	7,463
$N_h = 5$	17,985	17,265	59,850	13,183

5. Conclusion

This work presents the development of a novel Newton-Krylov iterative method within a multi-harmonic balance and pseudo-arclength continuation algorithm to efficiently compute the time-periodic motions of large-scale, nonlinear mechanical systems. The algorithm uses pseudo-arclength continuation to trace the periodic orbits of the harmonically excited equations. An inexact Newton method is used to determine the approximate corrections and predictions of the system, and these approximations are calculated using Krylov subspace iterative solvers. Two methods are combined to efficiently solve for the sequence of linear systems from the predictor and corrector steps, namely the delayed frequency preconditioner, and the GCRO-DR iterative solver with Krylov subspace recycling. Both methods recycle data from previous linear systems along the solution branch, providing overall cost savings within the solver. The recycled preconditioner is only refactorized when the performance of the iterative solver deteriorates. Krylov subspace recycling uses harmonic Ritz vectors from the previous linear system and provides an initial subspace for the solution of the next linear system. This enables improvements in the performance of the iterative solver by requiring fewer iterations to satisfy the approximate solution to the desired numerical tolerance.

Two example problems with contact type nonlinearities demonstrate the performance of the iterative solver strategy. Within each model, the non-restarted GMRES and GCRO-DR solver are utilized, along with four variants of preconditioners, namely LU factorization, two versions of iLU preconditioning (zero fill-in and Crout version), and a block-diagonal preconditioner with Crout iLU factorization. In many of the cases presented, the iterative solvers provided favorable speedups compared to the direct solver, but certain combinations of solvers and preconditioner led to worse performance. The best performance observed is for the C-Beam model with Jenkins elements, in which there is a 12.05x reduction in solver cost when using BD-iLUC and non-restarted GMRES. It was observed that the use of subspace recycling improves the computational performance only when using a less accurate preconditioner. When the preconditioner accurately represents the system matrix, there is no observed acceleration in the convergence of the solver, and it was more advantageous to use the non-restarted GMRES solver without subspace recycling.

Krylov subspace iterative solvers are known to provide significant speedups when solving large-scale linear systems, and the performance is highly dependent on the problem of interest along with the type of preconditioner and solver. This study demonstrates how these techniques can be effectively leveraged to speed up calculations associated with multi-harmonic balance and continuation algorithms. Future studies will be motivated by the generalized framework in which other solvers and preconditioners can be explored to achieve even better improvements in solver performance.

Acknowledgements

This paper describes objective technical results and analysis. Any subjective views or opinions that might be expressed in the paper do not necessarily represent the views of the U.S. Department of Energy or the United

States Government. Supported by the Laboratory Directed Research and Development program at Sandia National Laboratories, a multimission laboratory managed and operated by National Technology and Engineering Solutions of Sandia LLC, a wholly owned subsidiary of Honeywell International Inc. for the U.S. Department of Energy's National Nuclear Security Administration under contract DE-NA0003525.

The authors would like to thank Christopher Van Damme for the many technical discussions and suggestions regarding multi-harmonic balance. The authors appreciate discussions with Daniel Rixen who suggested the idea to explore subspace recycling concepts within iterative solvers. Finally, the authors would like to thank Mike Parks for his help understanding and deploying the GCRO-DR solver.

Declarations

Conflict of interest: The authors declare that they have no conflict of interest.

Funding: provided in submission

Availability of data and material: N/A

Code availability: N/A

Authors' contributions: provided in submission

Ethics approval: N/A

Consent to participate: N/A

Consent for publication: N/A

References

[1] A. H. Nayfeh and D. T. Mook, *Nonlinear Oscillations*. New York: John Wiley and Sons, 1979.

[2] G. Kerschen, M. Peeters, J. C. Golinval, and A. F. Vakakis, "Nonlinear normal modes. Part I. A useful framework for the structural dynamicist," *Mechanical Systems and Signal Processing,* vol. 23, no. 1, pp. 170-94, 2009, doi: 10.1016/j.ymssp.2008.04.002.

[3] A. F. Vakakis, "Non-linear normal modes (NNMs) and their applications in vibration theory: an overview," *Mechanical Systems and Signal Processing,* vol. 11, no. 1, pp. 3-22, 1997, doi: 10.1006/mssp.1996.9999.

[4] J. P. Thomas, E. H. Dowell, and K. C. Hall, "Modeling Viscous Transonic Limit Cycle Oscillation Behavior Using a Harmonic Balance Approach," *Journal of Aircraft,* vol. 41, no. 6, pp. 1266-1274, 2004, doi: 10.2514/1.9839.

[5] W. Yao and S. Marques, "Prediction of Transonic Limit-Cycle Oscillations Using an Aeroelastic Harmonic Balance Method," *AIAA Journal,* vol. 53, no. 7, pp. 2040-2051, 2015, doi: 10.2514/1.J053565.

[6] A. H. Nayfeh, D. T. Mook, and S. Sridhar, "Nonlinear analysis of the forced response of structural elements," *The Journal of the Acoustical Society of America,* vol. 55, no. 2, pp. 281-291, 1974. [Online]. Available: http://dx.doi.org/10.1121/1.1914499.

[7] A. H. Nayfeh, *Perturbation methods*. John Wiley & Sons, 2008.

[8] M. Krack and J. Gross, *Harmonic Balance for Nonlinear Vibration Problems*, 1st ed. Springer International Publishing, 2019.

[9] S. M. Filipov, I. D. Gospodinov, and I. Faragó, "Shooting-projection method for two-point boundary value problems," *Applied Mathematics Letters,* vol. 72, pp. 10-15, 2017.

[10] H. B. Keller, *Numerical solution of two point boundary value problems*. SIAM, 1976.

[11] E. L. Allgower and K. Georg, *Introduction to numerical continuation methods*. SIAM, 2003.

[12] R. Seydel, *Practical bifurcation and stability analysis*. Springer Science & Business Media, 2009.

[13] M. Urabe, "Galerkin's procedure for nonlinear periodic systems," *Archive for Rational Mechanics and Analysis,* Article vol. 20, no. 2, pp. 120-152, 1965, doi: 10.1007/BF00284614.

[14] L. Wang, Z.-R. Lu, and J. Liu, "Convergence rates of harmonic balance method for periodic solution of smooth and non-smooth systems," *Communications in Nonlinear Science and Numerical Simulation,* vol. 99, p. 105826, 2021/08/01/ 2021, doi: https://doi.org/10.1016/j.cnsns.2021.105826.

[15] J. Lu, X. Zhao, and S. Yamada, *Harmonic balance finite element method: applications in nonlinear electromagnetics and power systems*. John Wiley & Sons, 2016.

[16] Y. B. Kim and S. T. Noah, "Bifurcation analysis for a modified Jeffcott rotor with bearing clearances," *Nonlinear Dynamics,* vol. 1, no. 3, pp. 221-241, 1990/05/01 1990, doi: 10.1007/BF01858295.
[17] L. Peletan, S. Baguet, G. Jacquet-Richardet, and M. Torkhani, "Use and Limitations of the Harmonic Balance Method for Rub-Impact Phenomena in Rotor-Stator Dynamics," in *ASME Turbo Expo 2012: Turbine Technical Conference and Exposition*, 2012, vol. Volume 7: Structures and Dynamics, Parts A and B, pp. 647-655, doi: 10.1115/gt2012-69450. [Online]. Available: https://doi.org/10.1115/GT2012-69450
[18] L. Salles, B. Staples, N. Hoffmann, and C. Schwingshackl, "Continuation techniques for analysis of whole aeroengine dynamics with imperfect bifurcations and isolated solutions," *Nonlinear Dynamics,* vol. 86, no. 3, pp. 1897-1911, 2016/11/01 2016, doi: 10.1007/s11071-016-3003-y.
[19] G. Von Groll and D. J. Ewins, "The harmonic balance method with arc-length continuation in rotor/stator contact problems," *Journal of sound and vibration,* vol. 241, no. 2, pp. 223-233, 2001.
[20] C. Berthold, J. Gross, C. Frey, and M. Krack, "Development of a fully-coupled harmonic balance method and a refined energy method for the computation of flutter-induced Limit Cycle Oscillations of bladed disks with nonlinear friction contacts," *Journal of Fluids and Structures,* vol. 102, p. 103233, 2021.
[21] Y. Colaïtis and A. Batailly, "The harmonic balance method with arc-length continuation in blade-tip/casing contact problems," *Journal of Sound and Vibration,* vol. 502, p. 116070, 2021/06/23/ 2021, doi: https://doi.org/10.1016/j.jsv.2021.116070.
[22] C. M. Firrone, S. Zucca, and M. M. Gola, "The effect of underplatform dampers on the forced response of bladed disks by a coupled static/dynamic harmonic balance method," *International Journal of Non-Linear Mechanics,* vol. 46, no. 2, pp. 363-375, 2011.
[23] M. Krack, L. Panning-von Scheidt, J. Wallaschek, C. Siewert, and A. Hartung, "Reduced Order Modeling Based on Complex Nonlinear Modal Analysis and Its Application to Bladed Disks With Shroud Contact," *Journal of Engineering for Gas Turbines and Power,* vol. 135, no. 10, 2013, doi: 10.1115/1.4025002.
[24] L. Pesaresi, L. Salles, A. Jones, J. Green, and C. Schwingshackl, "Modelling the nonlinear behaviour of an underplatform damper test rig for turbine applications," *Mechanical Systems and Signal Processing,* vol. 85, pp. 662-679, 2017.
[25] R. Alcorta, S. Baguet, B. Prabel, P. Piteau, and G. Jacquet-Richardet, "Period doubling bifurcation analysis and isolated sub-harmonic resonances in an oscillator with asymmetric clearances," *Nonlinear Dynamics,* vol. 98, no. 4, pp. 2939-2960, 2019.
[26] S. Karkar, B. Cochelin, and C. Vergez, "A comparative study of the harmonic balance method and the orthogonal collocation method on stiff nonlinear systems," *Journal of Sound and Vibration,* vol. 333, no. 12, pp. 2554-2567, 2014/06/09/ 2014, doi: https://doi.org/10.1016/j.jsv.2014.01.019.
[27] A. Mélot, E. Rigaud, and J. Perret-Liaudet, "Bifurcation tracking of geared systems with parameter-dependent internal excitation," *Nonlinear Dynamics,* vol. 107, no. 1, pp. 413-431, 2022.
[28] T. Vadcard, A. Batailly, and F. Thouverez, "On Harmonic Balance Method-based Lagrangian contact formulations for vibro-impact problems," *Journal of Sound and Vibration,* vol. 531, p. 116950, 2022.
[29] J.-Y. Yoon and B. Kim, "Stability and bifurcation analysis of super- and sub-harmonic responses in a torsional system with piecewise-type nonlinearities," *Scientific Reports,* vol. 11, no. 1, p. 23601, 2021/12/08 2021, doi: 10.1038/s41598-021-03088-z.
[30] A. Givois, A. Grolet, O. Thomas, and J.-F. Deü, "On the frequency response computation of geometrically nonlinear flat structures using reduced-order finite element models," *Nonlinear Dynamics,* vol. 97, no. 2, pp. 1747-1781, 2019/07/01 2019, doi: 10.1007/s11071-019-05021-6.
[31] N. Jacques, E. M. Daya, and M. Potier-Ferry, "Nonlinear vibration of viscoelastic sandwich beams by the harmonic balance and finite element methods," *Journal of Sound and Vibration,* vol. 329, no. 20, pp. 4251-4265, 2010/09/27/ 2010, doi: https://doi.org/10.1016/j.jsv.2010.04.021.
[32] A. Opreni, N. Boni, R. Carminati, and A. Frangi, "Analysis of the Nonlinear Response of Piezo-Micromirrors with the Harmonic Balance Method," *Actuators,* vol. 10, no. 2, p. 21, 2021. [Online]. Available: https://www.mdpi.com/2076-0825/10/2/21.
[33] P. Ribeiro and M. Petyt, "GEOMETRICAL NON-LINEAR, STEADY STATE, FORCED, PERIODIC VIBRATION OF PLATES, PART I: MODEL AND CONVERGENCE STUDIES," *Journal of Sound and Vibration,* vol. 226, no. 5, pp. 955-983, 1999/10/07/ 1999, doi: https://doi.org/10.1006/jsvi.1999.2306.
[34] C. I. Van Damme, M. S. Allen, and J. J. Hollkamp, "Updating Geometrically Nonlinear Reduced-Order Models Using Nonlinear Modes and Harmonic Balance," *AIAA Journal,* vol. 58, no. 8, pp. 3553-3568, 2020.
[35] T. M. Cameron and J. H. Griffin, "An Alternating Frequency/Time Domain Method for Calculating the Steady-State Response of Nonlinear Dynamic Systems," *Journal of Applied Mechanics,* vol. 56, no. 1, pp. 149-154, 1989, doi: 10.1115/1.3176036.

[36] T. Detroux, L. Renson, L. Masset, and G. Kerschen, "The harmonic balance method for bifurcation analysis of large-scale nonlinear mechanical systems," *Computer Methods in Applied Mechanics and Engineering,* vol. 296, pp. 18-38, 2015/11/01/ 2015, doi: https://doi.org/10.1016/j.cma.2015.07.017.
[37] S. Narayanan and P. Sekar, "A FREQUENCY DOMAIN BASED NUMERIC–ANALYTICAL METHOD FOR NON-LINEAR DYNAMICAL SYSTEMS," *Journal of Sound and Vibration,* vol. 211, no. 3, pp. 409-424, 1998/04/02/ 1998, doi: https://doi.org/10.1006/jsvi.1997.1319.
[38] G. Xie and J. Y. K. Lou, "Alternating frequency/coefficient (AFC) technique in the trigonometric collocation method," *International Journal of Non-Linear Mechanics,* vol. 31, no. 4, pp. 531-545, 1996/07/01/ 1996, doi: https://doi.org/10.1016/0020-7462(96)00003-0.
[39] E. Petrov and D. Ewins, "Analytical formulation of friction interface elements for analysis of nonlinear multi-harmonic vibrations of bladed disks," *J. Turbomach.,* vol. 125, no. 2, pp. 364-371, 2003.
[40] L. Renson, G. Kerschen, and B. Cochelin, "Numerical computation of nonlinear normal modes in mechanical engineering," *Journal of Sound and Vibration,* vol. 364, pp. 177-206, 2016/03/03/ 2016, doi: https://doi.org/10.1016/j.jsv.2015.09.033.
[41] R. Barrett *et al.*, *Templates for the solution of linear systems: building blocks for iterative methods*. SIAM, 1994.
[42] Y. Saad, *Iterative methods for sparse linear systems*. SIAM, 2003.
[43] D. A. Knoll and D. E. Keyes, "Jacobian-free Newton–Krylov methods: a survey of approaches and applications," *Journal of Computational Physics,* vol. 193, no. 2, pp. 357-397, 2004/01/20/ 2004, doi: https://doi.org/10.1016/j.jcp.2003.08.010.
[44] R. Kouhia and M. Mikkola, "Some aspects on efficient path-following," *Computers & structures,* vol. 72, no. 4-5, pp. 509-524, 1999.
[45] R. S. Dembo, S. C. Eisenstat, and T. Steihaug, "Inexact newton methods," *SIAM Journal on Numerical analysis,* vol. 19, no. 2, pp. 400-408, 1982.
[46] M. Benzi, "Preconditioning techniques for large linear systems: a survey," *Journal of computational Physics,* vol. 182, no. 2, pp. 418-477, 2002.
[47] V. Rizzoli, F. Mastri, C. Cecchetti, and F. Sgallari, "Fast and robust inexact Newton approach to the harmonic-balance analysis of nonlinear microwave circuits," *IEEE Microwave and Guided Wave Letters,* vol. 7, no. 10, pp. 359-361, 1997.
[48] V. Rizzoli, F. Mastri, F. Sgallari, and G. Spaletta, "Harmonic-balance simulation of strongly nonlinear very large-size microwave circuits by inexact Newton methods," in *1996 IEEE MTT-S International Microwave Symposium Digest*, 1996, vol. 3: IEEE, pp. 1357-1360.
[49] Y. Saad and M. H. Schultz, "GMRES: A generalized minimal residual algorithm for solving nonsymmetric linear systems," *SIAM Journal on scientific and statistical computing,* vol. 7, no. 3, pp. 856-869, 1986.
[50] D. L. Rhodes and A. Gerasoulis, "Scalable parallelization of harmonic balance simulation," in *International Parallel Processing Symposium*, 1999: Springer, pp. 1055-1064.
[51] D. L. Rhodes and B. S. Perlman, "Parallel computation for microwave circuit simulation," *IEEE transactions on microwave theory and techniques,* vol. 45, no. 5, pp. 587-592, 1997.
[52] W. Dong and P. Li, "A parallel harmonic-balance approach to steady-state and envelope-following simulation of driven and autonomous circuits," *IEEE transactions on computer-aided design of integrated circuits and systems,* vol. 28, no. 4, pp. 490-501, 2009.
[53] N. Soveiko, M. S. Nakhla, and R. Achar, "Comparison study of performance of parallel steady state solver on different computer architectures," *IEEE transactions on computer-aided design of integrated circuits and systems,* vol. 29, no. 1, pp. 65-77, 2009.
[54] N. Soveiko, M. Nakhla, R. Achar, and E. Gad, "Scalable parallel matrix solver for steady state analysis of large nonlinear circuits," in *2008 IEEE MTT-S International Microwave Symposium Digest*, 2008: IEEE, pp. 1401-1404.
[55] A. Mehrotra and A. Somani, "A robust and efficient harmonic balance (HB) using direct solution of HB Jacobian," in *Proceedings of the 46th Annual Design Automation Conference*, 2009, pp. 370-375.
[56] W. Yao, J. M. Jin, and P. T. Krein, "A 3D finite element analysis of large-scale nonlinear dynamic electromagnetic problems by harmonic balancing and domain decomposition," *International Journal of Numerical Modelling: Electronic Networks, Devices and Fields,* vol. 29, no. 2, pp. 166-180, 2016.
[57] L. Han, X. Zhao, and Z. Feng, "An Adaptive Graph Sparsification Approach to Scalable Harmonic Balance Analysis of Strongly Nonlinear Post-Layout RF Circuits," *IEEE Transactions on Computer-Aided Design of Integrated Circuits and Systems,* vol. 34, no. 2, pp. 173-185, 2015, doi: 10.1109/TCAD.2014.2376991.
[58] J. Sánchez, M. Net, B. Garcıa-Archilla, and C. Simó, "Newton–Krylov continuation of periodic orbits for Navier–Stokes flows," *Journal of Computational Physics,* vol. 201, no. 1, pp. 13-33, 2004.
[59] M. Net and J. Sánchez, "Continuation of bifurcations of periodic orbits for large-scale systems," *SIAM Journal on Applied Dynamical Systems,* vol. 14, no. 2, pp. 674-698, 2015.

[60] I. Waugh, S. Illingworth, and M. Juniper, "Matrix-free continuation of limit cycles for bifurcation analysis of large thermoacoustic systems," *Journal of Computational Physics,* vol. 240, pp. 225-247, 2013.
[61] G. Formica, F. Milicchio, and W. Lacarbonara, "A Krylov accelerated Newton–Raphson scheme for efficient pseudo-arclength pathfollowing," *International Journal of Non-Linear Mechanics,* vol. 145, p. 104116, 2022.
[62] J. Sierra, P. Jolivet, F. Giannetti, and V. Citro, "Adjoint-based sensitivity analysis of periodic orbits by the Fourier–Galerkin method," *Journal of Computational Physics,* vol. 440, p. 110403, 2021.
[63] S. He, E. Jonsson, C. A. Mader, and J. R. Martins, "Coupled Newton–Krylov time-spectral solver for flutter and limit cycle oscillation prediction," *AIAA Journal,* vol. 59, no. 6, pp. 2214-2232, 2021.
[64] D. Zhou, Z. Lu, T. Guo, and G. Chen, "On the performance of harmonic balance method for unsteady flow with oscillating shocks," *Physics of Fluids,* vol. 32, no. 12, p. 126103, 2020.
[65] J. Blahoš, A. Vizzaccaro, L. Salles, and F. El Haddad, "Parallel harmonic balance method for analysis of nonlinear dynamical systems," in *Turbo Expo: Power for Land, Sea, and Air*, 2020, vol. 84232: American Society of Mechanical Engineers, p. V011T30A028.
[66] G. Jenovencio, A. Sivasankar, Z. Saeed, and D. Rixen, "AN DELAYED FREQUENCY PRECONDITIONER APPROACH FOR SPEEDING-UP FREQUENCY RESPONSE COMPUTATION OF STRUCTURAL COMPONENTS," in *XI International Conference on Structural Dynamics*, 2020.
[67] M. L. Parks, E. De Sturler, G. Mackey, D. D. Johnson, and S. Maiti, "Recycling Krylov subspaces for sequences of linear systems," *SIAM Journal on Scientific Computing,* vol. 28, no. 5, pp. 1651-1674, 2006.
[68] M. Bolten, N. Božović, and A. Frommer, "Preconditioning of Krylov subspace methods using recycling in Lattice QCD computations," *PAMM,* vol. 13, no. 1, pp. 413-414, 2013.
[69] L. Feng, P. Benner, and J. G. Korvink, "Subspace recycling accelerates the parametric macro-modeling of MEMS," *International Journal for Numerical Methods in Engineering,* vol. 94, no. 1, pp. 84-110, 2013.
[70] S. Keuchel, J. Biermann, M. Gehlken, and O. von Estorff, "Speed up of 3D-acoustics in frequency domain by the Fast Multipole Method in combination with Krylov Subspace Recycling based iterative solvers," in *AIA-DAGA 2013 Conference on Acoustics, EAA Euroregio/EAA Winter School*, 2013, pp. 18-21.
[71] S. Xu, S. Timme, and K. J. Badcock, "Enabling off-design linearised aerodynamics analysis using Krylov subspace recycling technique," *Computers & Fluids,* vol. 140, pp. 385-396, 2016.
[72] E. F. Yetkin and O. Ceylan, "Recycling Newton–Krylov algorithm for efficient solution of large scale power systems," *International Journal of Electrical Power & Energy Systems,* vol. 144, p. 108559, 2023.
[73] L. Zhu *et al.*, "GCRO-DR Method for Solving Three-Dimensional Electromagnetic Wave Scattering," in *2022 IEEE International Symposium on Antennas and Propagation and USNC-URSI Radio Science Meeting (AP-S/URSI)*, 2022: IEEE, pp. 1530-1531.
[74] H. Dai, Z. Yan, X. Wang, X. Yue, and S. N. Atluri, "Collocation-based harmonic balance framework for highly accurate periodic solution of nonlinear dynamical system," *International Journal for Numerical Methods in Engineering,* vol. 124, no. 2, pp. 458-481, 2023.
[75] M. Peeters, R. Viguié, G. Sérandour, G. Kerschen, and J. C. Golinval, "Nonlinear normal modes, Part II: Toward a practical computation using numerical continuation techniques," *Mechanical Systems and Signal Processing,* vol. 23, no. 1, pp. 195-216, 2009, doi: 10.1016/j.ymssp.2008.04.003.
[76] D. S. Watkins, *Fundamentals of matrix computations*. John Wiley & Sons, 2004.
[77] H.-B. An, Z.-Y. Mo, and X.-P. Liu, "A choice of forcing terms in inexact Newton method," *Journal of Computational and Applied Mathematics,* vol. 200, no. 1, pp. 47-60, 2007/03/01/ 2007, doi: https://doi.org/10.1016/j.cam.2005.12.030.
[78] S. C. Eisenstat and H. F. Walker, "Choosing the forcing terms in an inexact Newton method," *SIAM Journal on Scientific Computing,* vol. 17, no. 1, pp. 16-32, 1996.
[79] K. M. Soodhalter, E. de Sturler, and M. E. Kilmer, "A survey of subspace recycling iterative methods," *GAMM-Mitteilungen,* vol. 43, no. 4, p. e202000016, 2020, doi: https://doi.org/10.1002/gamm.202000016.
[80] G. Karypis and V. Kumar, "A Fast and High Quality Multilevel Scheme for Partitioning Irregular Graphs," *SIAM Journal on Scientific Computing,* vol. 20, no. 1, pp. 359-392, 1998, doi: 10.1137/s1064827595287997.
[81] P. Wriggers, T. Vu Van, and E. Stein, "Finite element formulation of large deformation impact-contact problems with friction," *Computers & Structures,* vol. 37, no. 3, pp. 319-331, 1990/01/01/ 1990, doi: https://doi.org/10.1016/0045-7949(90)90324-U.
[82] F. Pichler, W. Witteveen, and P. Fischer, "A complete strategy for efficient and accurate multibody dynamics of flexible structures with large lap joints considering contact and friction," *Multibody System Dynamics,* vol. 40, no. 4, pp. 407-436, 2017/08/01 2017, doi: 10.1007/s11044-016-9555-2.
[83] R. R. J. Craig and M. C. C. Bampton, "Coupling of Substructures for Dynamic Analysis," *AIAA Journal,* vol. 6, no. 7, pp. 1313-1319, 1968, doi: 10.2514/3.4741.

[84] W. C. Hurty, "Vibrations of structural systems by component mode synthesis," *Journal of the Engineering Mechanics Division,* vol. 86, no. 4, pp. 51-70, 1960.
[85] B. R. Pacini, R. J. Kuether, and D. R. Roettgen, "Shaker-structure interaction modeling and analysis for nonlinear force appropriation testing," *Mechanical Systems and Signal Processing,* vol. 162, p. 108000, 2022/01/01/ 2022, doi: https://doi.org/10.1016/j.ymssp.2021.108000.
[86] Y. Chen, T. A. Davis, W. W. Hager, and S. Rajamanickam, "Algorithm 887: CHOLMOD, supernodal sparse Cholesky factorization and update/downdate," *ACM Transactions on Mathematical Software (TOMS),* vol. 35, no. 3, pp. 1-14, 2008.
[87] C. D. Team, "CUBIT 15.6 User Documentation," SAND2020-4156 W, Sandia National Laboratories, Albuquerque, NM, April 2020.
[88] S. S. D. D. Team, "Sierra/SD User's Manual 5.8," SAND2022-8168, Sandia National Laboratories, Albuquerque, NM, June 2022.
[89] S. Zucca and C. M. Firrone, "Nonlinear dynamics of mechanical systems with friction contacts: Coupled static and dynamic Multi-Harmonic Balance Method and multiple solutions," *Journal of Sound and Vibration,* vol. 333, no. 3, pp. 916-926, 2014/02/03/ 2014, doi: https://doi.org/10.1016/j.jsv.2013.09.032.
[90] T. A. Davis, "Algorithm 832: UMFPACK V4. 3---an unsymmetric-pattern multifrontal method," *ACM Transactions on Mathematical Software (TOMS),* vol. 30, no. 2, pp. 196-199, 2004.